AD-A285 456

AR-008-635

DSTO-RR-0001

Models to Estimate High Frequency Acoustic Scattering due to Thermal Fine- and Micro-Structure of the Ocean

R.A. Thuraisingham

DTIC
ELECTE
OCT 13 1994
S G D

APPROVED
FOR PUBLIC RELEASE

94-32079

© Commonwealth of Australia

DEPARTMENT OF DEFENCE
DEFENCE SCIENCE AND TECHNOLOGY ORGANISATION

Models to Estimate High Frequency Acoustic Scattering due to Thermal Fine- and Micro-Structure of the Ocean

R.A. Thuraisingham

DSTO Research Report
DSTO-RR-0001

Abstract

Existing models to obtain intensity and phase changes of sound due to thermal fluctuations in the ocean, such as that developed by Chernov, are limited in their application. They are valid only for an isotropic medium and where the range is much greater than the correlation distance of the fluctuations. Extensions to short range and for an anisotropic medium are described here, both for the stochastic wave and ray models. Theoretical expressions obtained for acoustic fluctuations are easily evaluated. Numerical estimates are provided using stochastic wave and ray models for certain parameters of range, frequency and temperature variation, of interest in target strength measurements. These estimates indicate acoustic fluctuations for an anisotropic medium are always higher than for an isotropic media. For a range of 100 m, frequency of 100 kHz and temperature fluctuation of 7×10^{-3} *C deg, the root mean square relative intensities and the root mean square phase fluctuations are on the average higher by a factor of 6, where the vertical correlation lengths are the same and the radial correlation length is about 50 times larger. Closed form expressions in the deterministic ray approximation are given to evaluate intensity and phase changes due to the mean temperature gradient. The validity of the deterministic ray theory results is discussed. Results from the stochastic wave and ray models are examined for the applicability of the stochastic ray model at high frequencies. At mega hertz frequencies and ranges of 1-3 metres, which are of interest in acoustic mine imaging, estimates of the phase fluctuations from the stochastic ray approximation and the wave model are indistinguishable. Theoretical expressions of the phase structure function are given in the ray approximation to provide estimates of the phase coherence between signals. These results can provide valuable comparisons with experimental results, when such measurements are carried out with frequencies in the mega hertz band and at ranges of 1-3 metres.*

DTIC QUALITY INSPECTED 5

DEPARTMENT OF DEFENCE
DSTO AERONAUTICAL & MARITIME RESEARCH LABORATORY

94 1 20

Published by

Aeronautical and Maritime Research Laboratory
GPO Box 4331
Melbourne Victoria 3001 Australia

Telephone: (03) 626 8111
Fax: (03) 626 8999
© Commonwealth of Australia 1994
AR No. 008-638

APPROVED FOR PUBLIC RELEASE

Author

R.A. Thuraisingham
Maritime Operations Division

R.A. Thuraisingham is a research scientist attached to Maritime Operations Division of AMRL in Sydney. He obtained his BSc degree in Chemistry and Mathematics from the University of Colombo, Sri Lanka in 1970, and his doctorate in molecular quantum mechanics from Cambridge University, UK in 1975. He has been at DSTO since 1989.

Accesion For
NTIS CRA&I ☒
DTIC TAB ☐
Unannounced ☐
Justification
By
Distribution /
Availability Codes
Dist | Avail and / or Special
A-1

Contents

1. INTRODUCTION 7

2. SOME EXPERIMENTAL TEMPERATURE AND TEMPERATURE GRADIENT PROFILES 9

3. DETERMINISTIC RAY THEORY RESULTS 14

4. STOCHASTIC WAVE AND RAY THEORY IN A RANDOM MEDIUM 20

4.1 *Correlation Function, Mean Square Scattered Pressure and Attenuation* 21

4.2 *Amplitude and Phase Fluctuations in Wave and Ray Theory* 26

4.3 *Numerical Estimates of Intensity and Phase Fluctuations for the Isotropic Correlation Function in the Wave and Ray Models* 29

4.4 *Numerical Estimates of Intensity and Phase Fluctuations for the Anisotropic Correlation Function in the Wave and Ray Models* 40

5. PHASE STRUCTURE FUNCTION USING STOCHASTIC RAY THEORY 42

6. SUMMARY 48

7. ACKNOWLEDGEMENTS 50

8. REFERENCES 51

APPENDIX – *List of Symbols* 52

Models to Estimate High Frequency Acoustic Scattering Due to Thermal Fine- and Micro-Structure of the Ocean

1. *Introduction*

Scattering in the ocean can result from several sources. These include organic and inorganic particles (such as plankton and sand), air bubbles, the sea bottom or surface, and changes in current or temperature. This paper focuses attention on high frequency acoustic scattering due to temperature changes in the ocean.

Scattering of sound due to temperature changes can cause attenuation and fluctuations in amplitude and phase. Amplitude fluctuations cause erratic detection of targets, since the targets tend to be detected when the signal is strong and lost when the signal is weak [Urick, 1983, p183]. Further, in acoustic underwater imaging, temperature fluctuations can cause varying intensities and phase errors at different positions of the image, and loss of correlation between signals. Thus the importance of this study.

In this paper a number of questions are looked at, in relation to high frequency acoustic scattering due to temperature changes in the ocean. How do we obtain reliable theoretical estimates of acoustic attenuation, intensity and phase fluctuations from ocean temperature measurements? Can we theoretically estimate intensity and phase fluctuations due to temperature changes in target strength measurements where the range is around 100 m? In the study of underwater acoustic imaging the range involved is a few metres. Is it possible to obtain theoretical estimates at this short range? The ocean being an anisotropic medium, how does one obtain estimates of acoustic fluctuations, since most of the models treat it as isotropic. How good is the stochastic ray approximation at frequencies of 100 kHz and above? An experiment usually carried out is the measurement of the coherence of the phases of an acoustic signal at two receivers separated in space. The phase structure function is a measure of this coherence. Is it possible to obtain theoretical estimates of this quantity at short range?

Flatte [1979, p93] presented the different sound transmission regions in the $\Lambda - \Phi$space. Here Λ is the diffraction parameter, and Φ the root mean square (rms) phase fluctuations in the ray model. These parameters are defined later in this report. Fig.1 is a diagram of this space. The unsaturated region corresponds to weak scattering, while the saturated region is that of strong scattering. The ray

region is where diffraction effects are small. For an isotropic medium expressions for Λ [Flatte, 1979, p91, eqn.6.2.3] and Φ^2 [Flatte, 1979, p92, eqn 6.2.5] are available. The expression for Φ^2 is valid only when the range (L) is very much greater than the correlation length (a_0).

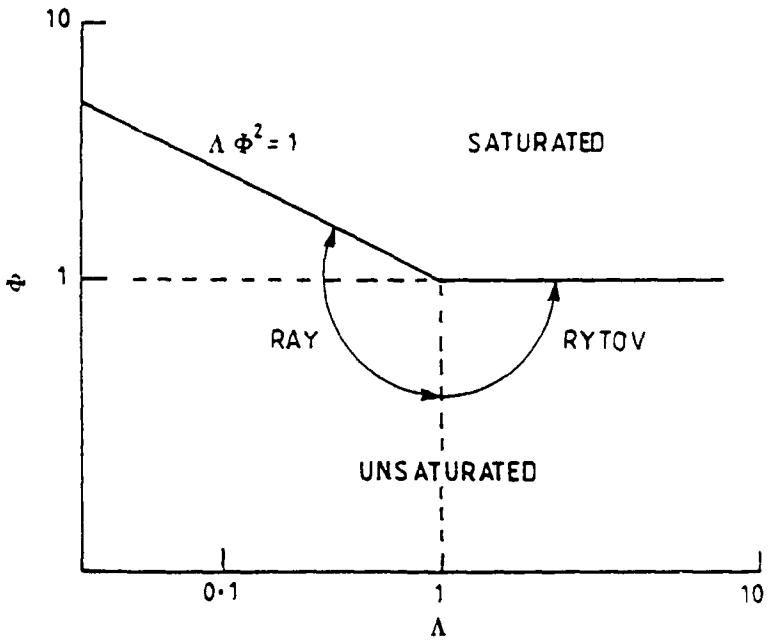

Figure 1: *Λ - Φ space, where Λ is the diffraction parameter, and Φ is the rms phase fluctuation in the ray model.*

In the ray region, expressions for the relative intensity fluctuations and phase fluctuations are available only for an isotropic medium, in a domain where L is very much greater than a_0 [Chernov, 1960, p34, p29; Flatte,1979, p92]. No closed form results are available for short range where L is less than or equal to a_0 and for an anisotropic medium. Again in the unsaturated Rytov region, expressions for relative intensity and phase fluctuations are available only for L very much greater than a_0 and for large $k_0 a_0$ [Chernov, 1960, p83]. No closed form expressions are available for L less than or equal to a_0, or for an anisotropic medium.

The paper discusses extensions to these models to obtain estimates of fluctuations at all ranges in the ray and Rytov regions, both for isotropic and anisotropic media. Numerical estimates are provided for some situations to give a measure of the magnitude of these fluctuations. Comparisons are made between the Chernov results and the results of the stochastic ray model. Mathematical detail is kept to a minimum; the emphasis will be on the application of models to obtain acoustic estimates.

The structure of the paper is as follows. Some experimental temperature and temperature gradient profiles are examined. Using deterministic ray theory, closed form results for intensity and phase changes, with reference to a medium where there is no temperature gradient, are given. These results provide a qualitative understanding of the effect of the mean temperature gradient on

acoustic transmission, and quantitative estimates of intensity and phase changes under certain limited conditions. Next, a statistical model based on wave theory is developed and examined. Theoretical expressions for the mean square scattered pressure, attenuation, intensity and phase variance at a point separated horizontally from the transmitter are given. Comparisons are made with other models such as the Chernov wave model and a new stochastic ray model. Finally a theoretical expression for the phase structure function based on the stochastic ray model is described.

Velocity fluctuations that occur in the ocean can be classified in general into three time scales [Anderson and Zahuranec, 1977, p135]. Velocity fluctuations that arise due to earth's rotation occur in time scales in excess of $1/f_i$ hours, where f_i is the inertial frequency or Coriolis frequency in hrs^{-1}. $1/f_i$ is approximately 24 hours. Velocity fluctuations that arise due to density gradient, stratification, or internal waves occur in time scales between $1/f_N$ to $1/f_i$, where f_N corresponds to the stability frequency or the Brunt Vaisala frequency ($1/f_N$ lies approximately between 30 mins to 24 hrs). Velocity fluctuations due to temperature fine structure and micro structure occur typically in a time scale less than 30 mins. The length scale of the structure is the basis of division between fine structure and micro structure. Fine structure corresponds to a length scale between 1 m and 100 m while for the micro structure it is below 1 m [Flatte, 1979, p15].

2. Some Experimental Temperature and Temperature Gradient Profiles

Fig. 2(a) is an example of a temperature profile obtained off Perth, Western Australia (from the RV Franklin). Fig. 2(b) is the corresponding temperature gradient profile. Temperature is given at every 2 m interval and has an accuracy of 10^{-3}C deg. The plots indicate that the temperature gradient has more structure than the temperature profile. In the next section it will be shown that it is the temperature gradient that is responsible for acoustic refraction.

Fig. 3(a) is an example of the temperature profile obtained at Woronora dam, a fresh water lake approximately 50 km south of Sydney, New South Wales. Fig. 3(b) is the temperature gradient of this profile. The profile is over a depth interval of 10 m. One can observe here some temperature inversions that are characteristic of surface layers. Normally, temperature decreases with depth ($dT/dZ < 0$). Fig. 4 shows the temperature variation with time over the same 10 m depth interval at three times. Plotted here is the temperature difference, that is the temperature at time t minus the temperature at t=0, where the temperature at t=0 corresponds to the profile shown in Fig. 3(a). The three parts of Fig. 4 correspond to variations after 3, 6 and 9 mins respectively. The diagram shows that even at the small time scales considered here there is a temperature variation, the magnitude of which on the average varies from 10^{-2} to 10^{-1}C deg per minute.

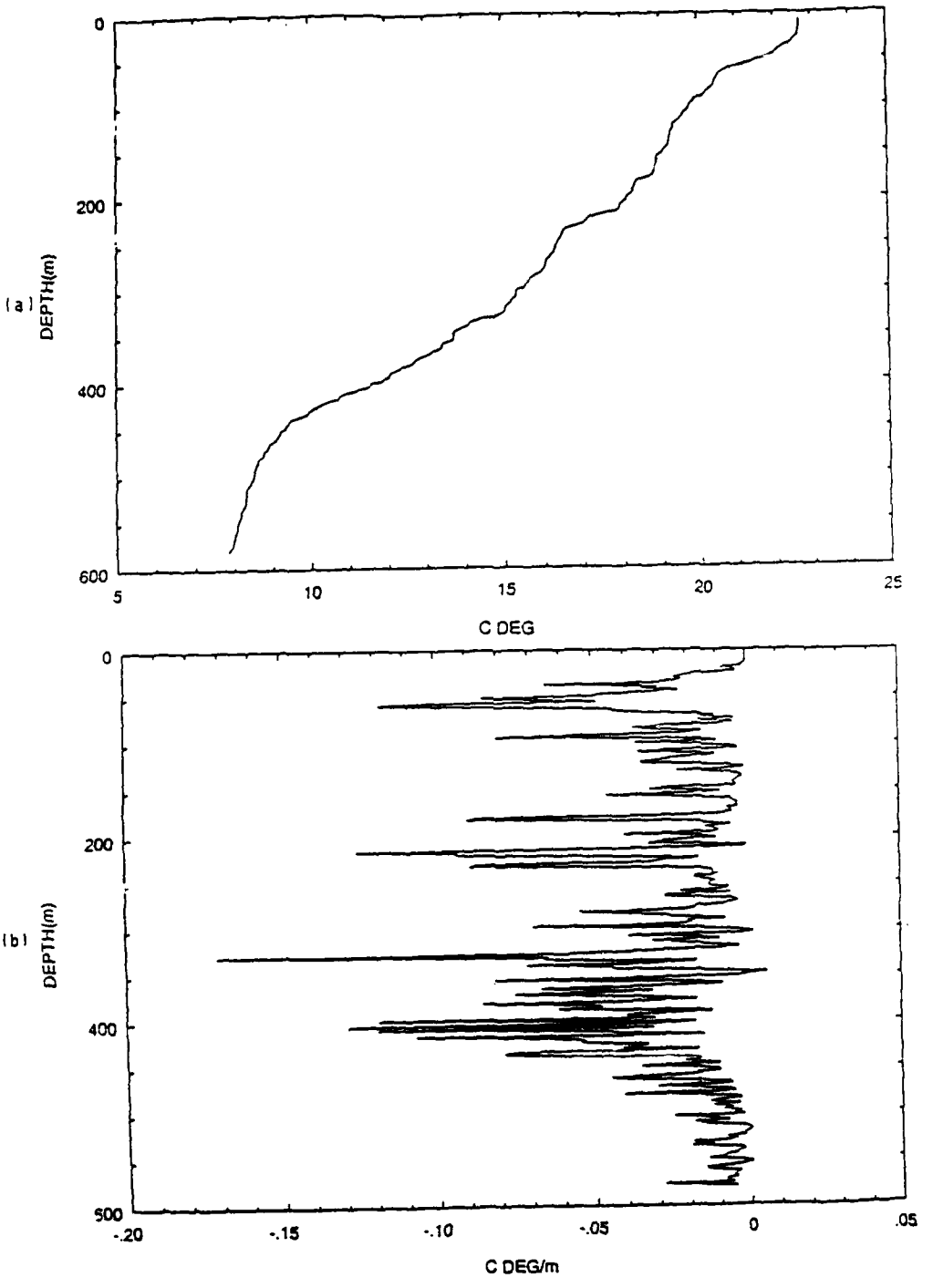

Figure 2: *Temperature, (b) Temperature gradient profile obtained off Perth in Western Australia, 31 58.82°S 115 11.42°E.*

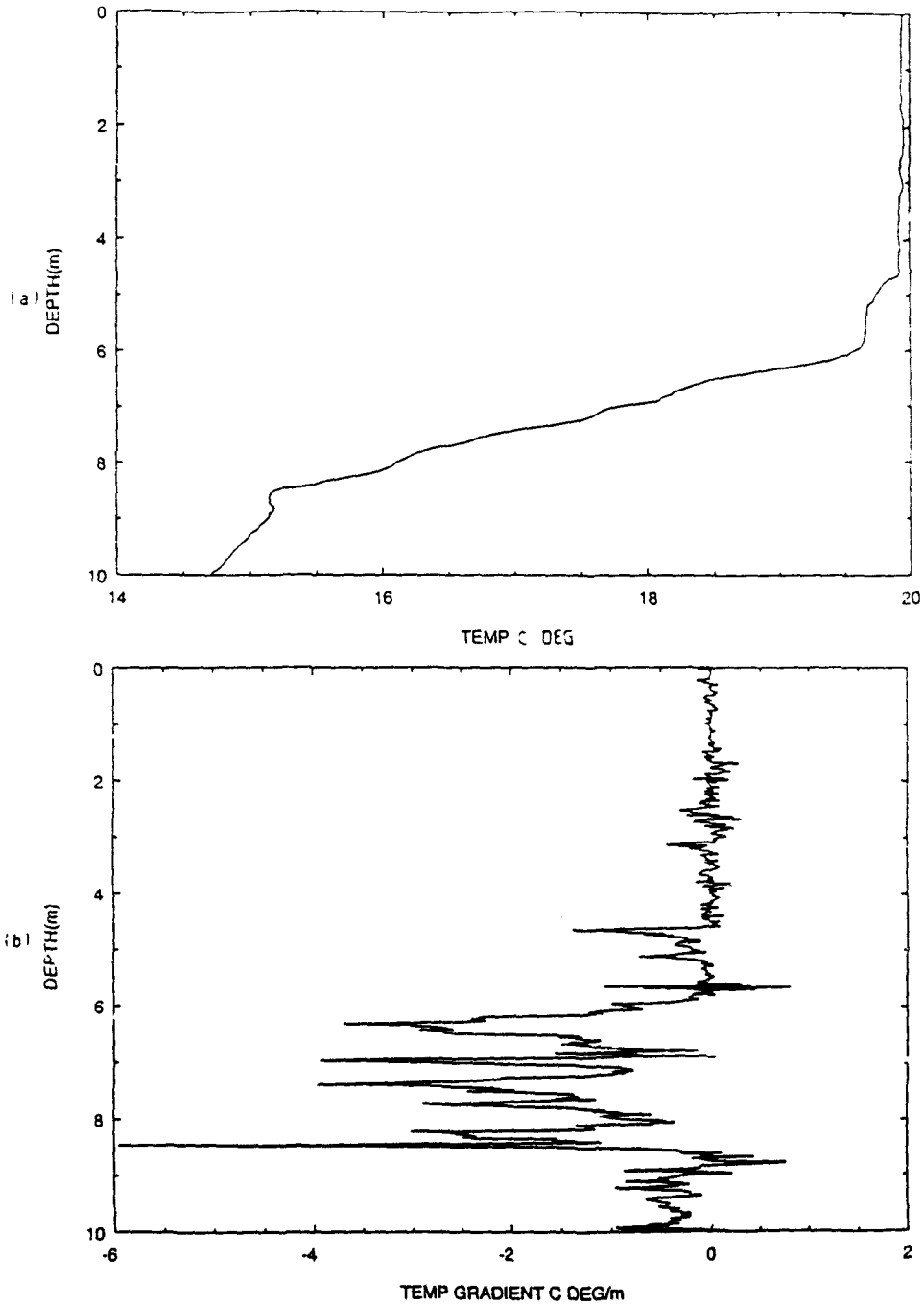

Figure 3: *(a) Temperature, (b) Temperature gradient profile obtained at Woronora dam, approximately 50 km south of Sydney, New South Wales.*

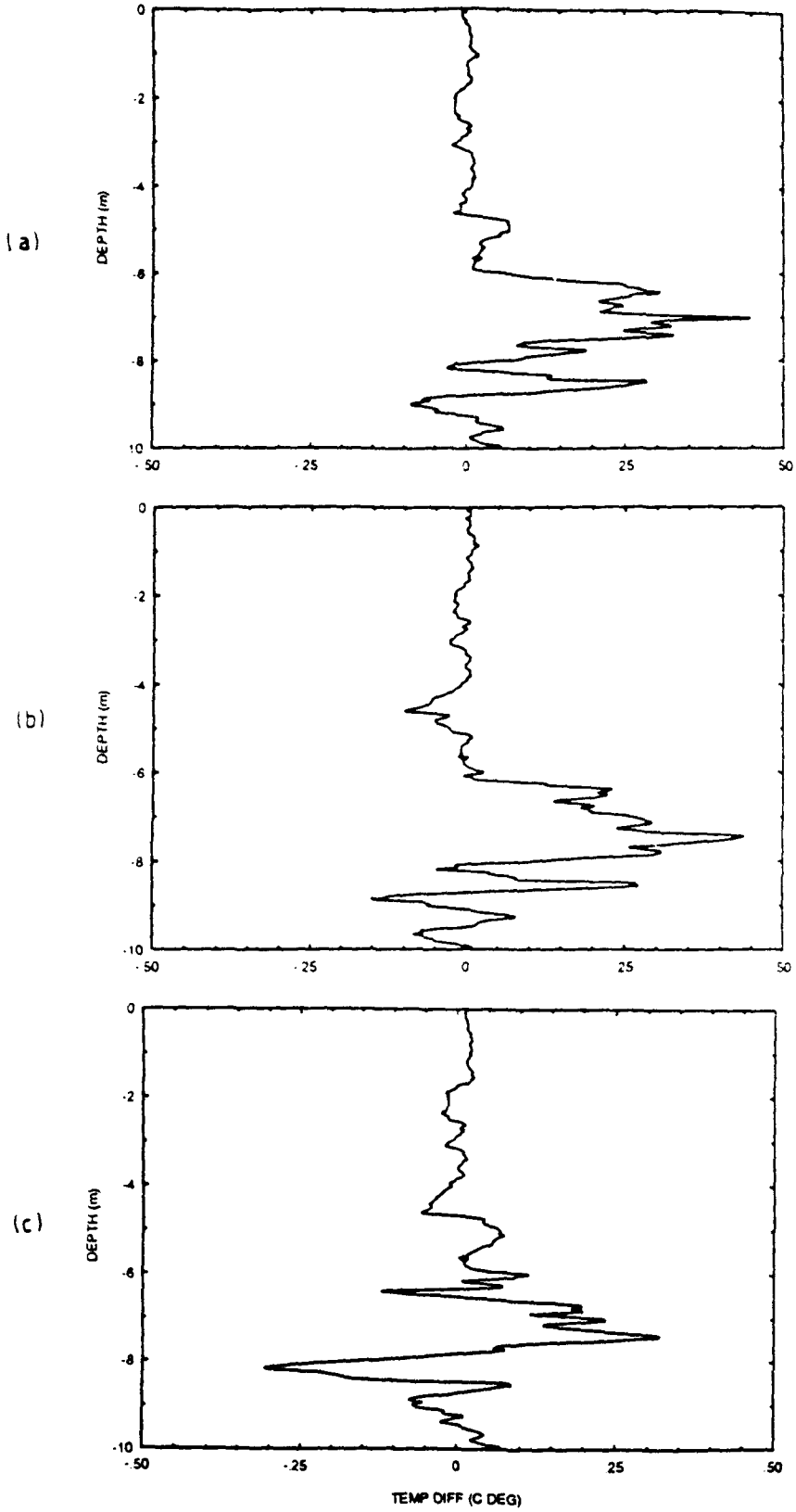

Figure 4: *Temperature difference observed at Woronora dam, after (a) 3 mins, (b) 6 mins, (c) 9 mins.*

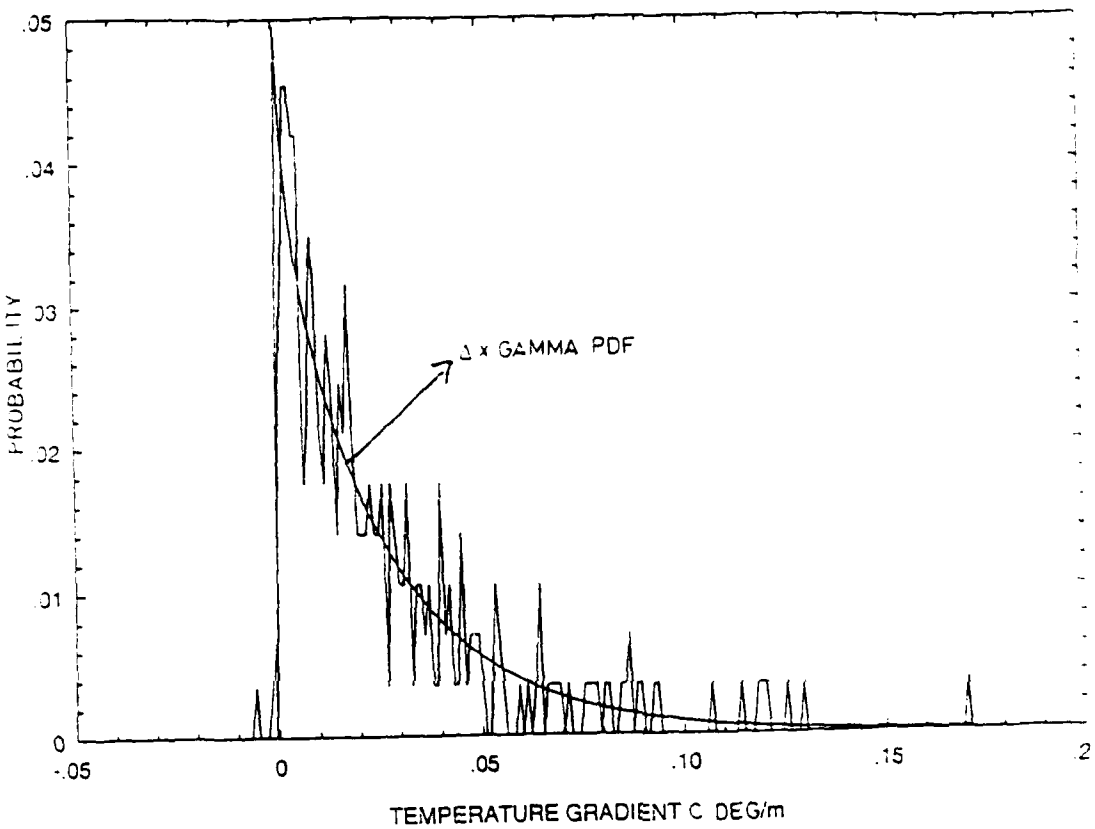

Figure 5: *Discrete probability function of the temperature gradient obtained off Perth in Western Australia, and Δ times the gamma probability density function (the smooth curve).* $\Delta = 10^{-3}$.

Fig. 5 is the discrete probability function of the temperature gradient obtained using the Perth data shown in Fig.2. This was obtained from the frequency of occurrence of a particular temperature gradient (using the Numerical Algorithm Group (NAG) routine G01AEF). For ease of comparison with the model of Hayes et al [1975], the temperature gradient plotted is the negative of the observed temperature gradient. The probability function shows a large skewness and can be fitted quite well to a function of the form $\Delta\ f(x)$, where Δ is the discretisation interval (equal to 10^{-3} in this example) and $f(x) = w_0 e^{\frac{-x}{\beta_0}} x^{\alpha_0 - 1}$, which is the gamma probability density function. The variable x corresponds to the temperature gradient. The mean and variance of the x distribution give the constants α_0 and β_0 [Freund, 1965, p147], while the result that the integral of the gamma probability density function over all values of x equals unity gives the

constant w_0. The model proposed by Hayes et al [1975] is the basis of the choice of $f(x)$. This model assumes layers of water that are nearly homogeneous, separated by sheets of sharp gradient with the mixing process occurring randomly in the vertical according to Poisson's law. This model is the basis of the choice of the anisotropic correlation function used later in this paper. So far, only vertical temperature profiles have been presented. However to obtain accurate estimates one also requires temperature profiles at horizontal separations.

Next, the effect of the mean temperature gradient on the acoustic intensity and phase changes will be examined, using simple deterministic ray theory. The reference is a medium where there is no temperature gradient.

3. *Deterministic Ray Theory Results*

The speed of sound (c)in the ocean can be given by an empirical equation of the form,

$$c = 1449.2 + 4.6T - 0.055T^2 + 0.0003T^3 + (1.34 - 0.012T)(S - 35) + 0.016Z$$

where T is the temperature in degrees Centigrade, S is the salinity in parts per thousand and Z the depth in metres [Medwin, 1975]. The speed of sound in the ocean is therefore a function of temperature, salinity and depth. However, as seen from the above equation the largest coefficient is that of temperature, which indicates that temperature change is the dominant cause of velocity variation.

Consider the case where we can approximate the above equation by $c = c_0 + gZ$ where g is equal to the velocity gradient $\frac{dc}{dZ}$. This g is mainly due to temperature variation. From ray theory, the path of the ray is given by [Officer, 1958, p48]:

$$\frac{d\theta}{ds} = p\frac{dc}{dZ}$$

where $p = \frac{\sin\theta_0}{c_0}$, s is the ray path, θ_0 the angle at the source, and c_0 the speed of sound near the source. We measure θ and θ_0 as the angles of the ray made with the vertical as shown in Fig. 6(a), with depth increasing downwards. If $\frac{dT}{dZ}$ changes with depth, then $\frac{dc}{dZ}$ changes with depth.

If $\frac{dc}{dZ} > 0$ then $\frac{d\theta}{ds} > 0$,

that is θ increases with s. In other words the ray bends upwards. On the other hand,

if $\frac{dc}{dZ} < 0$ then $\frac{d\theta}{ds} < 0$,

that is θ decreases with s, and the ray bends downwards. Thus due to temperature gradient, and therefore velocity gradient, rays undergo refraction.

Let us now look at intensity changes due to refraction. Suppose we have a receiver (R_1) and transmitter (T) at the same depth but separated horizontally by a distance L, as indicated in Fig. 6(a). Let us assume always that the transmitter is at $z = 0$ and the speed of sound near it is c_0. For a medium with a linear velocity gradient g, the intensity loss due to refraction measured in decibels (dB) is given by

$$\Delta I(R_1)(dB) = 10 Log_{10}(1 + \frac{g^2 L^2}{4 c_0{}^2}). \tag{1}$$

This was obtained from Officer's equations (2-83), (2-85) and from the expression for the intensity at horizontal range L given by,

$$I = \frac{E_0 \sin\theta_0}{L\cos\theta(\frac{\partial L}{\partial \theta_0})} \tag{2}$$

[Officer, 1958, p50, eqn.2-54]. In eqn(2), E_0 is the amount of energy emitted per unit time per unit solid angle. These equations are invalid for either L equal to 0 or for θ_0 equal to 0, as seen from Officer's eqns (2-54), (2-83) and (2-84). Equation (2) also fails at $\theta = 0.5\pi$, that is at a turning point. The intensity loss $\Delta I(R_1)$ is the difference in intensity at R_1, between a medium with a constant velocity gradient g and one where g=0. The larger the magnitude of g, the bigger is the intensity change. Another feature to be noted is that the intensity changes due to refraction, when receiver and transmitter are at the same horizontal distance, is independent of the sign of 'g'. What this means is that although the direction of bending is different, this being dependent on the sign of 'g', the amount of bending at R_1, that is the normal cross sectional area at R_1, is the same. To get an estimate for the intensity losses due to refraction, let us look at some results for $L = 100$ m and $c_0 = 1500$ m/s. The intensity loss for g equal to -0.23, -0.46 s^{-1} are $2.55 X 10^{-4}$ dB and $1.02 X 10^{-3}$ dB respectively. These results are obtained using eqn (1). The velocity gradients correspond to temperature gradients of -0.05 C deg/m and -0.1 C deg/m respectively. Such gradients are observable, as may be seen from Fig. 2(b).

Consider the case where the transmitter and receiver are separated by a distance R and at the same time they are displaced vertically by z. We again take a coordinate system where the depth increases downwards, so that if the receiver is above the transmitter, $z < 0$, while if the receiver is below the transmitter, $z > 0$. The intensity loss due to refraction in this case is given by,

$$\Delta I(R_2)(dB) = 10 \log_{10}(1 + \frac{g^2 R^2}{4 c_0^2} + \frac{gz}{c_0}) \tag{3}$$

When $z = 0$ and $R = L$, eqn (3) reduces to (1). The result given in eqn (3) is obtained using Officer's, eqn (2-89), (2-83) and (2-85). Both eqns (1) and (3) are invalid either for $L = 0$ or for $\theta_0 = 0$. Unlike eqn (1), for $z \neq 0$ the intensity loss depends on the sign of g. For $g < 0$ (velocity decreases with depth), intensity loss due to refraction will decrease with z for constant R. On the other hand for $g > 0$ (velocity increases with depth), intensity loss due to refraction will increase with z for constant R.

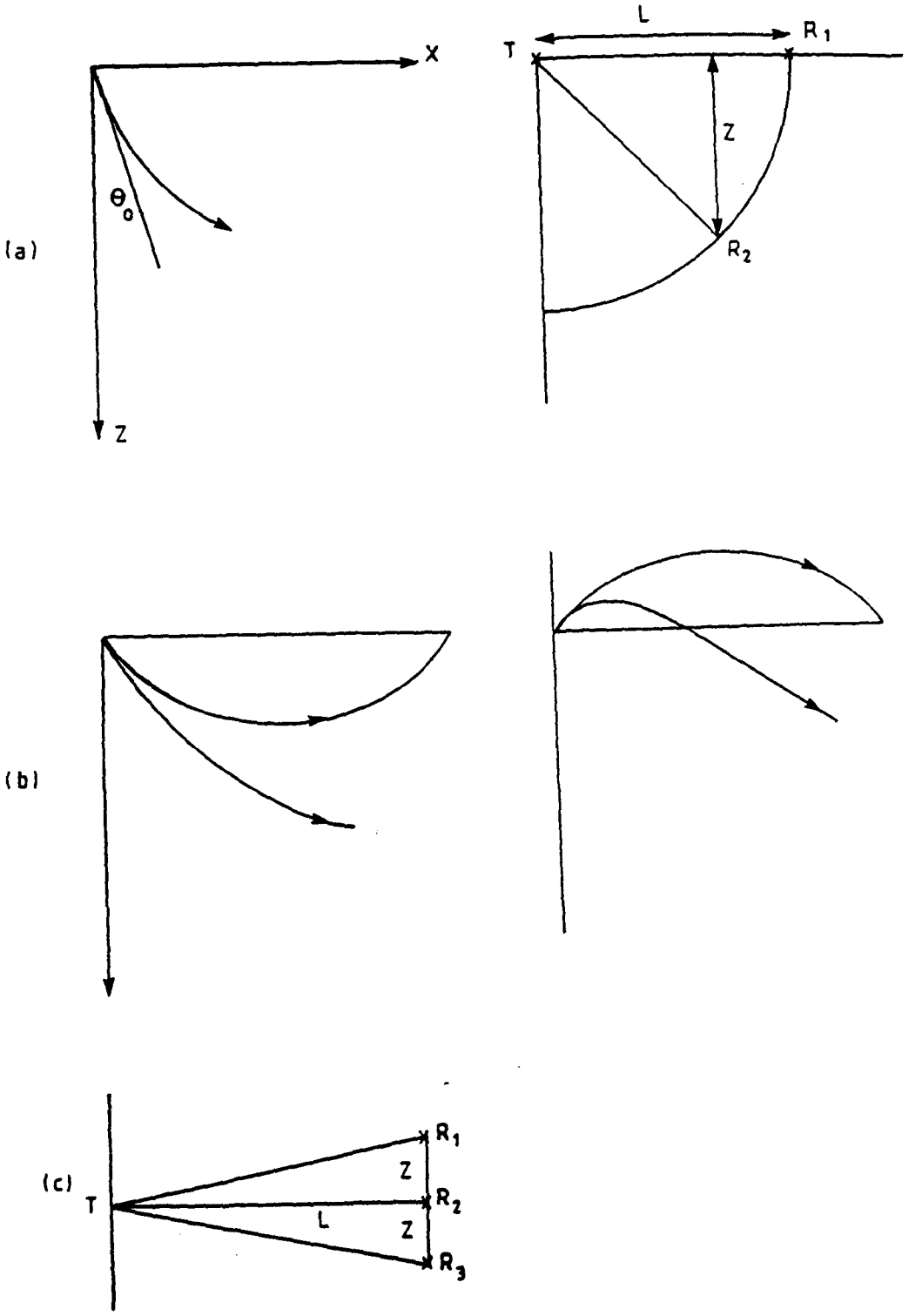

Figure 6: (a) Configuration of the system (b) ray paths (c) configuration of a system with 3 receivers.

An interesting corollary of eqn (3) is that one can find a depth z for a particular g and R where the intensity change due to refraction becomes zero. In other words the normal area of the ray tube is the same as that for an isospeed medium. This depth is given by

$$z = -\frac{gR^2}{4c_0}$$

For $g > 0$, this is above the transmitter, whereas for $g < 0$ it is below the transmitter.

Let us now consider the case of normal incidence where $\theta_0 = 0$. We begin with Officers eqn(2-81),

$$\frac{d\theta}{ds} = \frac{\sin\theta_0}{c_0} g \tag{4}$$

For $\theta_0 = 0$, the above expression becomes zero, which implies there is no refraction, and hence no intensity or phase changes due to refraction.

When $\theta_0 \neq 0$, but $L = 0$, Officer's eqn (2-83) and (2-85) gives $z = \frac{-2c_0}{g}$. In other words there is a unique position where the ray crosses the Z axis. At this position, using Officer's eqn (2-80), the acoustic velocity $c = -c_0$. Thus the situation with $\theta_0 \neq 0$, but $L = 0$ is not realistic.

Let us now look at the effect of the mean temperature gradient on the phase change, with reference to a medium where there is no temperature gradient. Consider the case where the transmitter and the receiver are at the same depth but separated horizontally by L. In this case derivation of a closed form result is possible. Starting from Officer's eqn (2-84), and using eqn (2-83), with the trigonometric relationship between the full and half angle for cotangent, one can show that the phase change due to refraction is

$$\Delta\phi(R_1) = (2\pi f)\left\{\frac{2}{g}\ln\left[\frac{Lg}{2c_0} + \left(\frac{L^2g^2}{4c_0^2} + 1\right)^{\frac{1}{2}}\right] - \frac{L}{c_0}\right\} \qquad g \neq 0$$

where f is frequency in Hz.

Consider $g = -g_1$. Substituting for g, one obtains after some algebra:

$$\Delta\phi(R_1) = (2\pi f)\left\{\frac{2}{g_1}\ln\left[\frac{Lg_1}{2c_0} + \left(\frac{L^2g_1^2}{4c_0^2} + 1\right)^{\frac{1}{2}}\right] - \frac{L}{c_0}\right\} \qquad g_1 > 0 \tag{5}$$

This shows that the phase change is independent of the sign of g. For small $|g|$,

$$\Delta\phi(R_1) \approx (2\pi f)\frac{L^2|g|}{4c_0{}^2}$$

showing that the larger the value of $|g|$, the bigger is the phase change. If $|g|$ is equal to 0, then there is of course no phase change due to refraction.

Consider the case where the transmitter and receiver are at a separation R but displaced vertically by z. The method to obtain phase change due to refraction is as follows. For a particular R and z one calculates,

$$\cot\theta_0 = \frac{R^2 g + 2zc_0}{2c_0(R^2 - z^2)^{1/2}}$$

This was obtained using Officer's eqns (2-51) and (2-83). Starting from Officer's eqn (2-84), and again expressing the cotangent of the half angles in terms of the full angles, the phase change is given by,

$$\Delta\phi(R_2) = (2\pi f)\left\{\frac{1}{g}\ln\left[\frac{\cot\theta_0 + (\cot^2\theta_0 + 1)^{1/2}}{\gamma\cot\theta + (\cot^2\theta + 1)^{1/2}}\right] - \frac{R}{c_0}\right\} \tag{6}$$

where from Officer's eqn (2-51),

$$\cot\theta = \frac{\left[\cot^2\theta_0 - \frac{g^2z^2}{c_0^2} - \frac{2gz}{c_0}\right]^{1/2}}{1 + \frac{gz}{c_0}}$$

Equations (5) and(6) are valid for $g \neq 0$. If $g = 0$ there is no refraction and hence no phase change. The parameter γ is defined as follows:

If $\quad (R^2 - z^2)^{1/2} > \frac{c_0}{g}\cot(\theta_0)$

then $\quad \gamma = -1 \quad$ if $\quad g > 0 \quad$ while $\quad \gamma = 1 \quad$ if $\quad g < 0.$

If $\quad (R^2 - z^2)^{1/2} < \frac{c_0}{g}\cot(\theta_0)$

then $\quad \gamma = 1 \quad$ if $\quad g > 0 \quad$ while $\quad \gamma = -1 \quad$ if $\quad g < 0.$

If $\quad (R^2 - z^2)^{1/2} = \frac{c_0}{g}\cot(\theta_0)$

then $\quad \gamma = 1, \quad$ and $\quad \theta = \pi/2$

For $z = 0$, one can show that eqn (6) reduces to eqn (5). For $z \neq 0$ the phase change is dependent on the sign of g. To understand this, let us look at the ray paths drawn in Fig. 6(b). When $g > 0$ the receiver is in a region where the velocity is greater than c_0. This would therefore shorten the time taken by the ray to reach the receiver, when compared to a medium where $g = 0$. This results in a negative phase change. As depth increases, so does the phase change, where the reference is a medium having a constant sound speed c_0. If $g < 0$, the velocity of sound near the receiver is less than that near the transmitter. This would increase the time taken to reach the receiver, when compared to a medium where $g = 0$. This

would result in a positive phase change. Increasing the depth increases the phase change.

The only discontinuity and singularity that occur in eqn (6) are at $\theta_0 = 0$ and $\theta = 0$ respectively. If $\theta_0 = 0$, it has been shown before that there is no refraction, and hence no phase change. If $\theta = 0$, but $\theta_0 \neq 0$, then from Officer's eqn (2-85), $z = \frac{-c_0}{g}$ This position corresponds to $c = 0$, which is not realistic. In other words, if $\theta_0 \neq 0$, then θ can never equal zero.

To get an estimate of the phase changes and intensity changes due to refraction let us look at the system depicted in Fig. 6(c). The system consists of three receivers, all at the same horizontal distance L, but vertically displaced by $-z, 0$, and z m. In imaging it is not intensity or phase change at one point that is important but the differences between them. The phase and intensity changes at each of the receivers R_1, R_2 and R_3 are calculated using eqns(1), (3), (5) and (6). Let us consider three cases. The first case corresponds to $L = 3$ m, $z = 0.5$ m, $f = 1$ MHz and $g = -0.23$. The intensity changes at R_1, R_2 and R_3 are $3.33X10^{-4}, 2.29X10^{-7}$, and $-3.33X10^{-4}$ dB respectively, while the phase changes are $-0.488, -1.11X10^{-4}$ and 0.488 radians respectively. The next case considered is $L = 10$ m, $z = 0.5$ m, $f = 100$ kHz and $g = -0.23$. The intensity changes at R_1, R_2 and R_3 are $3.36X10^{-4}, 2.55X10^{-6}$ and $-3.30X10^{-4}$ dB respectively, while the phase changes are $-0.161, -4.10X10^{-4}$, and 0.161 radians respectively. For the third case, increasing L to 100 m at 100 kHz gives intensity changes at R_1, R_2 and R_3 of $5.88X10^{-4}, 2.55X10^{-4}$ and $-7.77X10^{-5}$ dB respectively, while the phase changes are $-2.02, -0.41$ and 1.195 radians respectively.

The results described so far, for intensity and phase changes using ray theory, were obtained by considering the medium to be one where the speed of sound varies linearly with a constant gradient and is homogeneous horizontally. In a medium that consists of many vertical layers with different constant velocity gradients, it is impossible to obtain closed form expressions for intensity and phase changes. In the case where one can identify the presence of more than one layer, the solution is obtained by solving numerically Officer's eqns (2-83 to 2-85) for each layer. The ray solution is an exact solution of the wave equation at infinite frequency. At finite frequencies the ray solution is a good approximation to the wave equation if [Tolstoy and Clay, 1966, p52 and Officer, 1958, p39]

$$\frac{\nabla^2 A}{k_0{}^2 A} << 1$$

where $k_0 (= {}^{2\pi f}/_{c_0})$ is the wave number, A the amplitude and ∇^2 the Laplacian. The ray solution fails at caustics and shadow zones [Tolstoy and Clay, 1966, p57]. In a plane stratified medium, like the one assumed here, it also fails at turning points. Eqns (1), (3), (5), (6) are obtained under the assumption that there are no reflections or scattering from the boundaries, and no interference. Under such circumstances for a plane stratified medium the equation of a caustic is defined by $\frac{\partial L(z,\theta_0)}{\partial \theta_0} = 0$ [Kravtsov and Orlov, 1990, p137], where L is the horizontal range.That would be the equation of the caustic is also seen from eqn (2). Using Officer's eqns (2-83, 2-85) for L and differentiating with respect to θ_0, the equation for the caustic can be obtained. The equation obtained is an implicit equation in θ_0. For a single layer having a constant velocity gradient (as assumed here),

numerical solution indicates absence of caustics. This can also be shown analytically as follows. For a medium with constant velocity gradient the ray paths for different for different θ_0 are circular arcs that pass through the source with a horizontal range of $\frac{2c_0}{g}\cot\theta_0$. Since the horizontal range decreases monotonically with θ_0, ray paths with different θ_0 do not intersect.

For near horizontal rays, using Officer's eqns (2-27,2-46,2-83,2-85,2-13) and the assumption that $\frac{1}{A}\frac{\partial A}{\partial z}$ and $\frac{\partial\theta}{\partial L}$ are approximately zero, one can show that the ray solution will be a good approximation to the wave equation if

$$\frac{c_0^2}{4\pi^2 f^2 L^2} << 1$$

For steep rays (where z is large), assuming $\frac{1}{A}\frac{\partial A}{\partial L}, \frac{\partial\theta}{\partial L}$, and $\frac{\partial\theta}{\partial z}$ to be all approximately zero, one can show using Officer's eqns (2-27, 2-46) that the ray solution will be a good approximation to the wave equation if $f >> g$ [Tolstoy and Clay, 1966, p50].

So far in this section, expressions to obtain intensity and phase changes in a medium with a mean temperature gradient have been described. The reference has been a medium where there is no temperature gradient. The usefulness of these simple closed form expressions is that one can estimate changes in intensity and phase, due to changes in the mean temperature gradient, in regions where the ray solution is valid.

4. *Stochastic Wave and Ray Theory in a Random Medium*

In most cases in the real ocean one can write

$$c = c_0 + gz + small\ \ random\ \ part$$

The following sections look at obtaining acoustic estimates such as intensity and phase fluctuations, and attenuation from the random part of the sound velocity. This is done using both stochastic wave and ray models. The stochastic ray model suffers from many deficiencies, in that there is no frequency dependence for intensity loss, and ignores diffraction and interference. However it is an exact solution at infinite frequency. By comparing the results of the stochastic ray model, with that of the stochastic wave model, the region of applicability of the stochastic ray model for finite frequencies is examined.

4.1 *Correlation Function, Mean Square Scattered Pressure and Attenuation*

The basis of this model is the approach developed by Liu [1991] to obtain the mean square scattered pressure for a discrete random medium. A correlation function or a spectral function characterises the random medium. This is obtained from a large collection of temperature data and will be a function of the environment. The covariance N_2 is given by

$$N_2(r-r') = \overline{\mu^2} N(r-r'),$$

where the correlation coefficient N is defined as

$$N(r-r') = \left\langle \frac{\frac{\delta c}{c}(r,v)\frac{\delta c}{c}(r',v)}{(\frac{\delta c}{c}(r,v))^2} \right\rangle$$

and $\overline{\mu^2}$ as

$$\overline{\mu^2} = \left\langle \left[\frac{\delta c}{c}(r,v)\right]^2 \right\rangle.$$

The symbol $\langle\ \rangle$ indicates averaging over different temperature profiles, v. $\overline{\mu^2}$ is the mean square fractional speed fluctuation at position r. The spectral function is given by $\overline{\mu^2}F(\vec{K})$, where $F(\vec{K})$ is the Fourier transform of $N(r-r')$. $\vec{K} = (K_x, K_y, K_z)$, where $\vec{K}$ depends on the incident wave number k_0 and the direction of incident and scattered beam. In spherical coordinates,

$$\begin{aligned} K_x &= k_0(\sin\theta_i \cos\phi_i - \sin\theta_s \cos\phi_s) \\ K_y &= k_0(\sin\theta_i \sin\phi_i - \sin\theta_s \sin\phi_s) \\ K_z &= k_0(\cos\theta_i - \cos\phi_s) \end{aligned} \tag{7}$$

where i is the direction of the incident beam, and s the direction of the scattered beam. θ and ϕ are the polar and azimuthal angles respectively. For back-scattered pressure, $\vec{K} = 2\vec{k}_0$.

Two forms of correlation and spectral functions have been used to deal with temperature fluctuations that occur at the fine structure and micro structure level. One is isotropic that is characteristic of micro structure fluctuations, and the other is anisotropic and characteristic of fine structure fluctuations. The isotropic functions $F(\vec{K})$ and $N(x,y,z)$ are given by Liebermann [1951], Chernov [1960, p10],

$$F(\vec{K}) = \left(\frac{a_0^3}{8(\pi)^{3/2}}\right) e^{-a_0^2(K_x^2+K_y^2+K_z^2)/4}$$

$$N(x,y,z) = e^{-(x^2+y^2+z^2)/a_0^2} \tag{7a}$$

where a_0 is the correlation length.

The anisotropic functions $F(K)$ and $N(x,y,z)$ are given by Unni and Kaufman [1981],

$$F(\vec{K}) = [\frac{\rho^2 z_0}{4\pi^2 (K_z^2 z_0^2 + 1)}] e^{-\rho^2 K_\rho^2 / 4}$$

$$K_\rho^2 = K_x^2 + K_y^2$$

$$N(x,y,z) = e^{-|z|/z_0} e^{-(x^2+y^2)/\rho_0^2} \tag{7b}$$

where z_0 is the correlation distance in the depth direction and ρ_0 is the correlation distance in the radial direction. The form of the anisotropic function is obtained from a statistical model where the thermal fine structure in the vertical is a steppy Poisson process and where the layered fine structure is advected horizontally and vertically by internal waves. The basis of the steppy Poisson process is the experimental discrete probability function of the observed layer size [Joyce and Desaubies, 1977]. The introduction of a steppy Poisson process in the vertical introduces the exponential function in the anisotropic correlation function. However it must be noted that the exponential function introduces a peculiarity, namely its partial derivative with respect to z at the origin differs from zero. This implies that the refractive index fluctuation is a discontinuous function [Chernov, 1960, p9]. The exponential function is commonly used however because it often yields realistic results. The parameters a_0, z_0, ρ_0 and $\overline{\mu^2}$ are dependent on the environment.

For a medium where the mean speed of sound is c_0, and where the sound source is continuous and monochromatic, the mean square scattered pressure at a distance r, very much greater than the dimensions of the scattering region of volume V, is given by [Chernov, 1960, p51]

$$\overline{|p_s(r)|^2} = \frac{A_0{}^2 k_0^4 \overline{\mu^2} (2\pi) V}{r^2} F(\vec{K}) \tag{8}$$

where $k_0 = \frac{\omega}{c_0}$, and ω, A_0 are the angular frequency and amplitude of the sound wave respectively.

Assuming the initial direction of the incident beam to be along the X axis, $\theta_i = 90°$ and $\phi_i = 0°$ let us evaluate the term

$$F_1(\vec{K}) = \frac{k_0^4}{(K_z^2 z_0^2 + 1)} e^{-\rho^2 K_\rho^2 / 4} \tag{9}$$

for the anisotropic function and

$$F_1(\vec{K}) = k_0^4 e^{-a_0^2 (K_x^2 + K_y^2 + K_z^2)/4} \tag{10}$$

for the isotropic function. The function $F_1(K)$ contains all the angular and the frequency dependence of the mean square scattered pressure. Fig. 7(a) is a plot of the anisotropic F_1 (eqns 7, 9) as a function of ϕ_s at 1 MHz for two scattering directions $\theta_s = 89.8°$ and $89.6°$. F_1 is plotted on a logarithmic scale with $\rho_0 = 74$ m, and $z_0 = 2$ m [Unni and Kaufman, 1981 and Joyce and Desaubies, 1977]. These lengths were obtained for the Sargasso sea, and are not universal parameters. From Fig. 7(a) we observe that in going from 89.8° to 89.6° there is a large decrease in the magnitude of F_1. Also, the function decreases very rapidly with increasing azimuthal scattering angle ϕ_s. This indicates that scattering is confined to a small angle close to the direction of propagation.

Fig. 7(b) is a plot of the anisotropic F_1 (eqns 7,9) for a particular scattered direction $\theta_s = 89.8°$ as a function of ϕ_s, for the two different frequencies 1 MHz and 100 kHz. The results indicate that as the frequency decreases scattering spreads over a wide angle. However the spread is still small, the function decreasing rapidly with increasing ϕ_s.

Fig. 7(c) is a plot of the isotropic F_1 (eqns 7,10) as a function of the azimuthal scattering angle ϕ_s, for the two angles $\theta_s = 89.9°$ and $89.8°$, with $a_0 = 0.7$ m. Changing the scattered direction from the incident direction of propagation, there is a marked decrease in F_1. However the width of the scattered beam using the isotropic spectral function is much greater than for the anisotropic function. The above results indicate that high frequency ($\lambda << a_0$) scattering is strongly directional, the direction being close to the direction of propagation, [Chernov, 1960, p52].

Next the evaluation of the total attenuation both for the isotropic and anisotropic functions is undertaken. Starting from equations (50), (51) and (52) of Chernov [1960, pp53, 54], the attenuation (α) is given by,

$$\alpha = \int_0^{\pi} \sin\theta d\theta \int_0^{2\pi} d\varphi \overline{|p_s(r)|^2} \frac{r^2}{A_0{}^2 V}. \tag{11}$$

The expression for $\overline{|p_s(r)|^2}$ is given by eqn (8). For the isotropic correlation function it is independent of the direction of propagation and can be easily evaluated, [Chernov, 1960, p55]:

$$\alpha(dB/m) = 4.34\overline{\mu^2} k_0{}^2 a_0 \sqrt{\pi}(1 - e^{-a_0^2 k_0^2}) \tag{12}$$

At high frequencies it varies as $k_0{}^2$. This arises since for large $k_0, k_0 a_0 >> 1$, and thus $e^{-a_0{}^2 k_0^2} \to 0$. Fig. 8(a) shows the attenuation in dB/m (eqn 12) at the two frequencies 1 MHz and 100 kHz, as a function of a_0 for $\overline{\mu^2} = 5.1X10^{-10}$. This $\overline{\mu^2}$ corresponds to a root mean square temperature fluctuation of $7X10^{-3}$ C deg. Although with increase in frequency, scattering becomes confined to a small region close to the direction of propagation, the increase in attenuation at small angles, causes the total attenuation to increase.

In the anisotropic case, attenuation will depend on the direction of propagation. Where the direction of propagation is along the Z axis, the attenuation is given by

$$\alpha(dB/m) = 4.34\overline{\mu^2} k_0^4 \rho_0^2 z_0 \int_0^{\pi} d\theta \sin\theta \frac{e^{-0.25\rho_0^2 k_0^2 \sin^2\theta}}{[k_0^2 z_0^2 (1-\cos\theta)^2 + 1]} \tag{13}$$

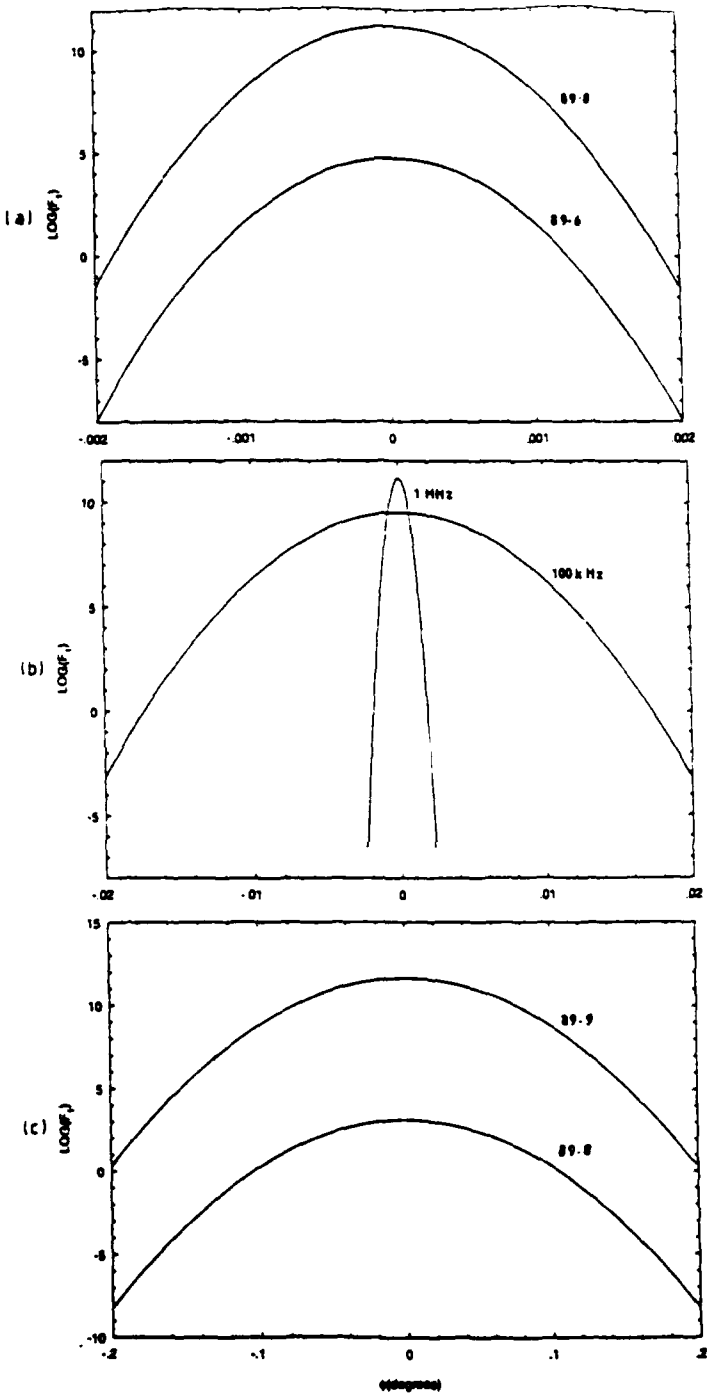

Figure 7: (a) Plot of F_1 (eqns. 7, 9) as a function of the azimuthal angle ϕ_s for 1 MHz and θ_s = 89.8° and 89.6°, (b) Plot of F_1 (eqns. 7, 9) as a function of ϕ_s for θ_s = 89.8°, and frequency of 1 MHz and 100 kHz. The spectral function is anisotropic, with ρ_0 = 74 m, and z_0 = 2 m. (c) Plot of F_1 (eqns. 7, 10) as a function of ϕ_s for θ_s = 89.9° and 89.8° at 1 MHz. a_0 = 0.7 m.

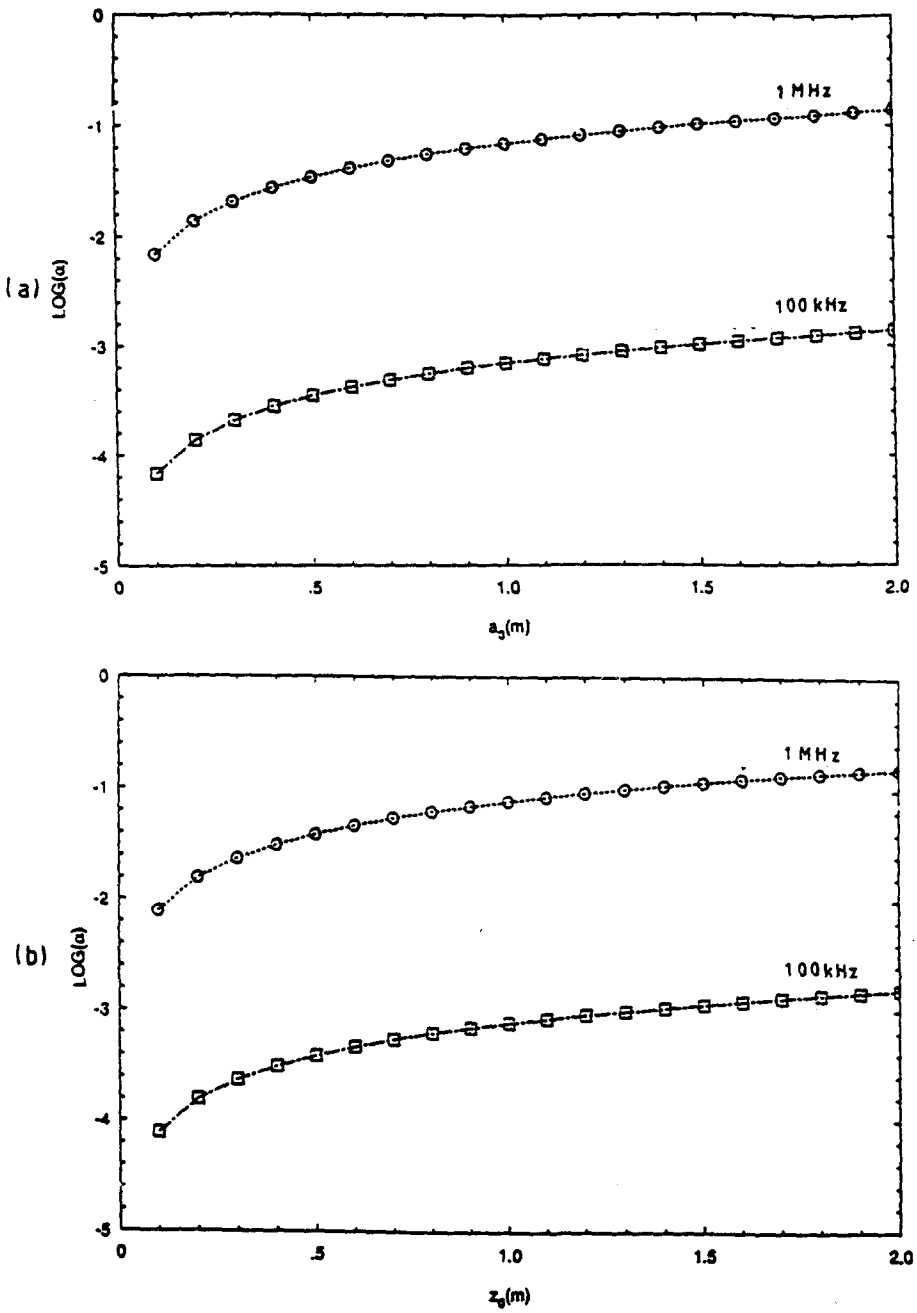

Figure 8: (a) Attenuation (α) in dB/m (eqn. 12) at 1 MHz and 100 kHz as a function of a_0. $\overline{\mu^2} = 5.1 \times 10^{-10}$. (b) Attenuation (α) in dB/m (eqn. 13) at 1 MHz and 100 kHz as a function of z_0 for the anisotropic function. $\rho_0 = 50$ m, $\overline{\mu^2} = 5.1 \times 10^{-10}$.

Integration over angles in the above integral arises due to scattering being in all directions. The integral is evaluated numerically using the NAG routine D01GAF. Since high frequency scattering is confined close to the direction of propagation, in this sector a fine interval has to be employed to obtain accurate results for attenuation. To obtain a relative error of less than 1%, for θ upto 0.1 radians, integration intervals were found to be of 10^{-3} radians and 10^{-4} radians at frequencies of 100 kHz and 1 MHz respectively. Beyond 0.1 radians a much coarser interval is used. Fig. 8(b) shows the attenuation (eqn 13) at 1 MHz and 100 kHz as a function of the vertical correlation length z_0 for $\rho_0 = 50$ m and $\overline{\mu^2} = 5.1 \times 10^{-10}$. The magnitudes are of the same order as the isotropic function and show a k_0^2 dependence. There is negligible variation with ρ_0. With propagation along the vertical Z direction, and attenuation being confined to angles close to the direction of propagation, the radial correlation length is expected to have a negligible effect.

4.2 *Amplitude and Phase Fluctuations in Wave and Ray Theory*

In the last section we found high frequency acoustic scattering confined to regions close to the direction of propagation. This effect indicates amplitude and phase fluctuations will become important. This section looks at obtaining estimates of these fluctuations. Consider an experiment where the receiver is in the direction of propagation and separated by a distance L from the source, which transmits a continuous wave monochromatic signal. The receiver receives the direct wave as well as waves scattered by the media. The superposition of the direct and scattered waves gives rise to fluctuations in the received signal. The Rytov method, [Chernov, 1960, p61] is used to obtain estimates of the mean square log amplitude fluctuations $\overline{(\ln(A/A_0))^2}$ and the mean square phase fluctuations, $\overline{(\Delta\phi)^2}$. Here A, A_0 are the amplitudes and ϕ, ϕ_0 the phase of the received and transmitted signals respectively. $\Delta\phi$ equals $\phi - \phi_0$. The Rytov method is applicable when the relative amplitude change, and phase change over a wavelength is small. There is no restriction on the total change of these quantities. Consider the source being placed at (0, 0, 0) and the receiver at (L, 0, 0). Then, following Chernov [1960, p70], we have:

$$\overline{(\ln(A/A_0))^2} = 0.5 k_0^2 \overline{\mu^2} (I_1 - I_2) \tag{14}$$

$$\overline{(\Delta\phi)^2} = 0.5 k_0^2 \overline{\mu^2} (I_1 + I_2), \tag{15}$$

where I_1, I_2 are integrals that depend on the correlation coefficient and are defined by Chernov [1960, p70]. Let us evaluate the integrals I_1, I_2 for the two different correlation coefficients.

For the isotropic correlation function,

$$I_1 = L^2 \int_0^1 dx \int_{-x}^{(1-x)} dy \frac{e^{-L^2 y^2 / a_0^2}}{\left[1 + 4L^2 y^2 / k_0^2 a_0^4\right]} \tag{16}$$

$$I_2 = L^2 \int_0^1 dx \int_{-x}^{1-x} dy \frac{e^{-L^2y^2/a_0^2}}{\left[1 + 4L^2(2-2x-y)^2/k_0^2a_0^4\right]} \tag{17}$$

These are obtained by starting from equations (118) and (119) of Chernov [1960, p70] and without making any further approximations (such as $L >> a_0$ or $ka_0 >> 1$).

Making the approximation that $L >> a_0$ and $ka_0 >> 1$, Chernov obtained, see his eqns (159), (160) in Chernov [1960, p83],

$$\overline{(\ln(\frac{A}{A_0}))^2} = 0.5\sqrt{\pi}\,\overline{\mu^2}k_0^2a_0L(1 - \frac{1}{D}\arctan(D)) \tag{18}$$

$$\overline{(\Delta\phi)^2} = 0.5\sqrt{\pi}\,\overline{\mu^2}k_0^2a_0L(1 + \frac{1}{D}\arctan(D)) \tag{19}$$

where $D = \frac{4L}{k_0a_0^2}$

In the limit $k_0a_0 \to \infty$ one can obtain simple analytical results. In this case,

$$I_1 \to \sqrt{\pi}a_0[L\ erf(\frac{L}{a_0}) + (e^{-L^2/a_0^2} - 1)\frac{a_0}{\sqrt{\pi}}] \tag{20}$$

where $erf(x)$ is the error function of argument x. For $k_0a_0 >> 1$, using eqns (16) and (17),

$$I_1 - I_2 \approx \frac{4L^4}{k_0^2a_0^4}\int_0^1 dx \int_{-x}^{1-x} dy\ e^{L^2y^2/a_0^2}[(2-2x-y)^2 - y^2] \tag{21}$$

In the limit $k_0a_0 \to \infty$, $I_1 - I_2 \to 0$ and therefore,

$$\overline{(\Delta\phi)^2} \to \overline{\mu^2}k_0^2\sqrt{\pi}a_0[L\ erf(\frac{L}{a_0}) + (e^{-L^2/a_0^2} - 1)\frac{a_0}{\sqrt{\pi}}] \tag{22}$$

One can also obtain this result from ray statistics, using the expression for the mean square transit time fluctuation given in Chernov [1960, p29]. Substituting the expression for $(I_1 - I_2)$ (eqn(21)), into eqn (14) the relative intensity fluctuation at large k_0a_0 becomes,

$$\overline{(\ln(A/A_0))^2} \to \frac{2\overline{\mu^2}L^4}{a_0^4}\int_0^1 dx \int_{-x}^{1-x} dy\ e^{-L^2y^2/a_0^2}[(2-2x-y)^2 - y^2] \tag{23}$$

There is no restriction on the value of the horizontal range in the above equation. When $L/a_0 >> 1$, eqn (22) becomes,

$$\overline{(\Delta\phi)^2} \rightarrow \overline{\mu^2} k_0^2 L \sqrt{\pi} a_0 \tag{24}$$

Chernov obtained the same result in the ray approximation, using the isotropic gaussian correlation function and evaluating the integral given in Chernov [1960, p29]. When $L/a_0 >> 1$, eqn (23) reduces to

$$\overline{(\ln(A/A_0)^2)} \rightarrow \frac{8\sqrt{\pi}}{3} \overline{\mu^2} \frac{L^3}{a_0^3} \tag{25}$$

Eqn (25) is the same as that obtained by Chernov in the ray approximation, [Chernov, 1960, p34]. Clearly his expressions in the ray model are therefore valid only when $L >> a_0$.

If $L/a_0 << 1$, eqn (22) reduces to,

$$\overline{(\Delta\phi)^2} \rightarrow 2\overline{\mu^2} k_0^2 L^2 \tag{26}$$

For the anisotropic correlation function, equations (118) and (119) of Chernov [1960, p 70] are again the starting point for the evaluation of the integrals I_1 and I_2. When evaluated without invoking any simplifications, one obtains for the integral I_1

$$I_1 = L^2 \int_0^1 dx \int_x^{1-x} dy \; e^{-L^2 y^2 / \rho_0^2} [IA(b_1, \rho_0) IC(b_1, z_0) + IB(b_1, \rho_0) ID(b_1, z_0)] \tag{27}$$

where $b_1 = k_0 / 2L|y|$.

The expression for the integral I_2 is given by

$$I_2 = L^2 \int_0^1 dx \int_{-x}^{1-x} dy \; e^{-y^2 L^2 / \rho_0^2} [IA(b_2, \rho_0) IC(b_2, z_0) + IB(b_2, \rho_0) ID(b_2, z_0)] \tag{28}$$

where $b_2 = k_0 / 2L(2 - 2x - y)$.

IA, *IB*, *IC* and *ID* are given by,

$$IA(b, \rho_0) = \sqrt{\frac{\sqrt{1/\rho_0^4 b^2 + 1} - 1/\rho_0^2 b}{1 + 1/\rho_0^4 b^2}}$$

$$IB(b, \rho_0) = \sqrt{\frac{\sqrt{1/\rho_0^4 b^2 + 1} + 1/\rho_0^2 b}{1 + 1/\rho_0^4 b^2}} \tag{29}$$

$$IC(b,z_0) = (\cos(q)(0.5 - S(q)) - \sin(q)(0.5 - C(q))$$

$$ID(b,z_0) = (\cos(q)(0.5 - C(q)) + \sin(q)(0.5 - S(q)) \tag{30}$$

in which $q = \frac{0.25}{z_0^2 b}$.

$S(q)$ and $C(q)$ are the Fresnel sine and cosine integrals, where

$$S(q) = \frac{1}{\sqrt{2\pi}} \int_0^q t^{-0.5} \sin(t)dt$$

$$C(q) = \frac{1}{\sqrt{2\pi}} \int_0^q t^{-0.5} \cos(t)dt$$

In the limit $k_0\rho_0 \to \infty, I_1 - I_2 \to 0$, with I_1 being the same as eqn (20) except that ρ_0 replaces a_0. Chernov has not treated the anisotropic case. Equations (16), (17), (27) and (28) do not have any restriction on the range or frequency, and are applicable at all ranges and frequencies.

4.3 *Numerical Estimates of Intensity and Phase Fluctuations for the Isotropic Correlation Function in the Wave and Ray Models*

In this section the isotropic correlation function is used to obtain some numerical estimates for intensity and phase fluctuations at high frequencies. The dependence of the estimates on the isotropic correlation length (a_0), $\overline{\mu^2}$, frequency (f), and range(L) is examined. Also, wave model results are compared with the results from the Chernov model and the statistical ray model. A brief discussion on the trends observed in the simulation results is given. A frequency of 100 kHz and a range close to 100 m are often used in target strength measurement of mines. This is the reason for the choice of these values for frequency and range in most of the calculations presented in this section.

In Fig. 9(a), comparisons of the rms relative intensity fluctuation (eqns (14, 16 and 17)) and the rms phase fluctuations (eqns (15, 16 and 17)) are made with the Chernov result (eqns (18) and (19)), as a function of range. The NAG routines D01AJF and D01GAF are used for the numerical evaluation of the inner and outer integrals in I_1 and I_2 respectively. Using a relative error of 10^{-7} for the inner integral and an interval of $5X10^{-3}$ for the outer integral, a relative error of less than 1% is achieved for the double integral. The parameters used in the comparison are $f = 100$ kHz, a_0=2 m and $\overline{\mu^2}$=5.1X10^{-10}. The value of $\overline{\mu^2}$ corresponds to a rms temperature fluctuation of 7X10^{-3}C deg and $k_0a_0 \sim 838 >> 1$. The plot shows that for L greater than 50 m, there is an error of less than 5% in the intensity between the results of Chernov and the wave model. At large range where L is very much greater than a_0 both models agree. In Fig. 9(b) comparison is made between the models as a function of k_0a_0. This is carried out with $L = 100$ m, $f = 100$ kHz, and $\overline{\mu^2} = 5.1X10^{-10}$. The maximum value of

a_0 used is 0.75 m, thus $L >> a_0$. The plot shows that the two models agree only for $k_0 a_0 >> 80$.

Figure 10 compares the rms relative intensity and rms phase obtained from the ray model (eqns (23, 22)) with that of the Chernov ray model (eqns(25, 24)), as a function of range L. The parameters used are $f = 200$ kHz, $\overline{\mu^2} = 5.1X10^{-10}$, $a_0 = 2$ m, and $k_0 a_0 = 1676$. Figure 10(a) compares the rms relative intensities and Fig. 10(b) compares the rms phases. The graphs indicate that the Chernov ray model results agree with our ray model results with an error of less than 5% only for L greater than 20 m. At this value of L, $L/a_0 = 10$. In other words the Chernov ray model (eqns (25, 24)), is valid only for L very much greater than a_0.

In Fig 11(a) the rms relative intensity fluctuations (eqns (14, 16, 17)), and in Fig. 11(b) the rms phase fluctuations (eqns (15, 16, 17)), are plotted for different isotropic correlation lengths a_0, with $f = 100$ kHz, $L = 100$ m, and $\overline{\mu^2} = 5.1X10^{-10}$.The correlation length a_0 varies from 10 cm to 2 m. The integrals (eqns (16, 17)) are evaluated numerically as before. The maximum variation in the rms relative intensity for this range of a_0 is less than 0.3 dB and the maximum phase fluctuation about 0.15 radians. The peak observed around 0.5 m in the rms intensity curve is interesting, and this is discussed later, along with the trend observed in the fluctuations as a function of a_0.

Figure 12(a) shows the variation of the rms relative intensity fluctuations (eqns (14, 16, 17)) for different $\overline{\mu^2}$. The variation in $\overline{\mu^2}$ corresponds to a variation in the rms temperature fluctuation from $7X10^{-3}$ to $3X10^{-2}$ C deg at a particular depth and salinity. Fig. 12(b) shows the variation in the rms phase (eqns (15, 16, 17)). The rms relative intensity fluctuation varies by about 1.2 dB and the rms phase fluctuation by about 0.3 radians over this interval of temperature fluctuation. The calculations are carried out with $f = 100$ kHz, $a_0 = 0.7$ m and $L = 100$ m. We have plotted the results here on a semi-logarithmic scale due to the range involved in $\overline{\mu^2}$. However if we plot it on a linear scale against $(\overline{\mu^2})^{0.5}$, a linear dependence is observed with the rms relative intensity and phase fluctuations, in accordance with eqns (14) and (15) respectively.

Figures 13(a) and (b) show the variation of the rms relative intensity fluctuations (eqns (14, 16, 17)) and rms phase fluctuations, (eqns (15, 16, 17)) as a function of frequency, where the frequency varies from 100 kHz to 400 kHz. The parameters used in the calculation are $\overline{\mu^2} = 5.1X10^{-10}$, $a_0 = 0.7$ m and $L = 100$ m. The rms relative intensity fluctuations initially show a non linear variation with frequency, but as the frequency increases, a linear dependence is seen. Simulations carried out at high frequencies show that the relative intensity approaches the result of eqn (25), where it will be independent of frequency. This is expected since $L >> a_0$ in this example. The rms phase fluctuation on the other hand, exhibits a linear variation even in the frequency range of 100 kHz to 400 kHz (it follows the trend predicted by either eqn (22) or (24)). This indicates that for phase fluctuations, agreement with the ray result can be obtained at a lower frequency.

Figures 14(a) and (b) show the variation of the rms relative intensity fluctuations (eqns (14, 16, 17)) and rms phase fluctuations (eqns (15, 16, 17)) as a function of range L, where the range varies from 50 m to 300 m. Other parameters taken for the calculations are $\overline{\mu^2} = 5.1X10^{-10}$, $a_0 = 0.7$ m and $f = 100$ kHz. The rms relative intensity shows a near linear relationship. In the ray approximation it varies as L^3 (eqn (25)), showing that the frequency has to be much higher for this limit to be reached. The rms phase fluctuations initially show a non linear

behaviour of $L^{0.5}$, becoming linear with increase in range. In the ray approximation the variation with range is non linear and is of the form $L^{0.5}$ (eqn (24)). It will be seen later that for a particular frequency, the smaller the range, the better is the agreement with the ray result.

Figure 15(a) compares the rms phase fluctuations obtained from the stochastic ray model (eqn (22)), with the wave model (eqns (15, 16, 17)), as a function of $k_0 a_0$. The calculations are carried out with $L = 100$ m and $\overline{\mu^2} = 5.1X10^{-10}$. The differences between the two models decrease with increase in $k_0 a_0$. Since the stochastic ray model is obtained from the wave model in the limit $k_0 a_0 \rightarrow \infty$, the observed results follow the expected trend.

The correlation distance is a measure of the decay length of the coherence of fluctuations. The bigger the length the larger the distance at which fluctuations become uncorrelated. For a range greater than a_0, the larger the value of a_0, more time is spent in going through the coherent region of fluctuations. This increases the phase fluctuations, as seen also from eqn (24). On the other hand if the range is much smaller than a_0 we would expect the phase fluctuations to be independent of a_0, as seen also from eqn (26).

Variation of intensity fluctuation with correlation length is more involved than the variation of phase fluctuations. To understand this let us consider Fig. 1. The diffraction or the size parameter Λ is given by [Flatte, 1979, eqn.6.2.3],

$$\Lambda = \frac{L}{6 a_0^2 k_0} \tag{31}$$

The strength parameter Φ is the rms phase fluctuation in the ray approximation and is given by eqn (22).The geometrical approximation or the ray model is valid when diffraction effects are small, that is $\Lambda < 1$ and $\Lambda\Phi^2 < 1$. The Rytov method is applicable for $\Lambda > 1$ but $\Lambda\Phi^2 \leq 1$. Fig. 16(a) is a plot of the diffraction parameter (eqn (31)), as a function of a_0, for $f = 100$ kHz and $L = 100$ m. The plots indicate that diffraction becomes important for a_0 less than 0.5 m. We observed before that the maximum in the rms intensity as a function of a_0 occurred close to 0.5 m. The Fresnel zone radius is defined as the size of the inhomogeneities that will cause the scattered path length from source to receiver to differ from the unscattered path length by half a wavelength. When this happens there will be interference between the direct and scattered rays. At 100 kHz over a path length of 100 m, this is evaluated and is equal to 0.5 m. This is close to the value of a_0 at which the maximum in the rms relative intensity occurred (see Fig.11(a)).

Figure 16(b) is a plot of Φ the rms phase fluctuation obtained in the ray approximation, given by eqn (22), as a function of a_0. Figure 16(c) is a plot of $\Lambda\Phi^2$ as a function of a_0. Correlation length (a_0) varies from 10 cm to 2 m. Other parameters used in the calculations are $\overline{\mu^2} = 5.1X10^{-10}$, $f = 100$ kHz and $L = 100$ m. The results indicate that we are in the unsaturated region of the $\Lambda - \Phi$ space. Unlike the rms phase fluctuations, intensity fluctuations decrease with correlation distance. Since diffraction effects decrease with increase in correlation length, the ray model becomes a good approximation to evaluate fluctuations at large correlation length. In the geometric approximation intensity fluctuations decrease with increase in the correlation length [Chernov, 1960, p34]. We would therefore expect the same trend in the results of intensity fluctuations from the wave model. This trend is seen in Fig.11(a).

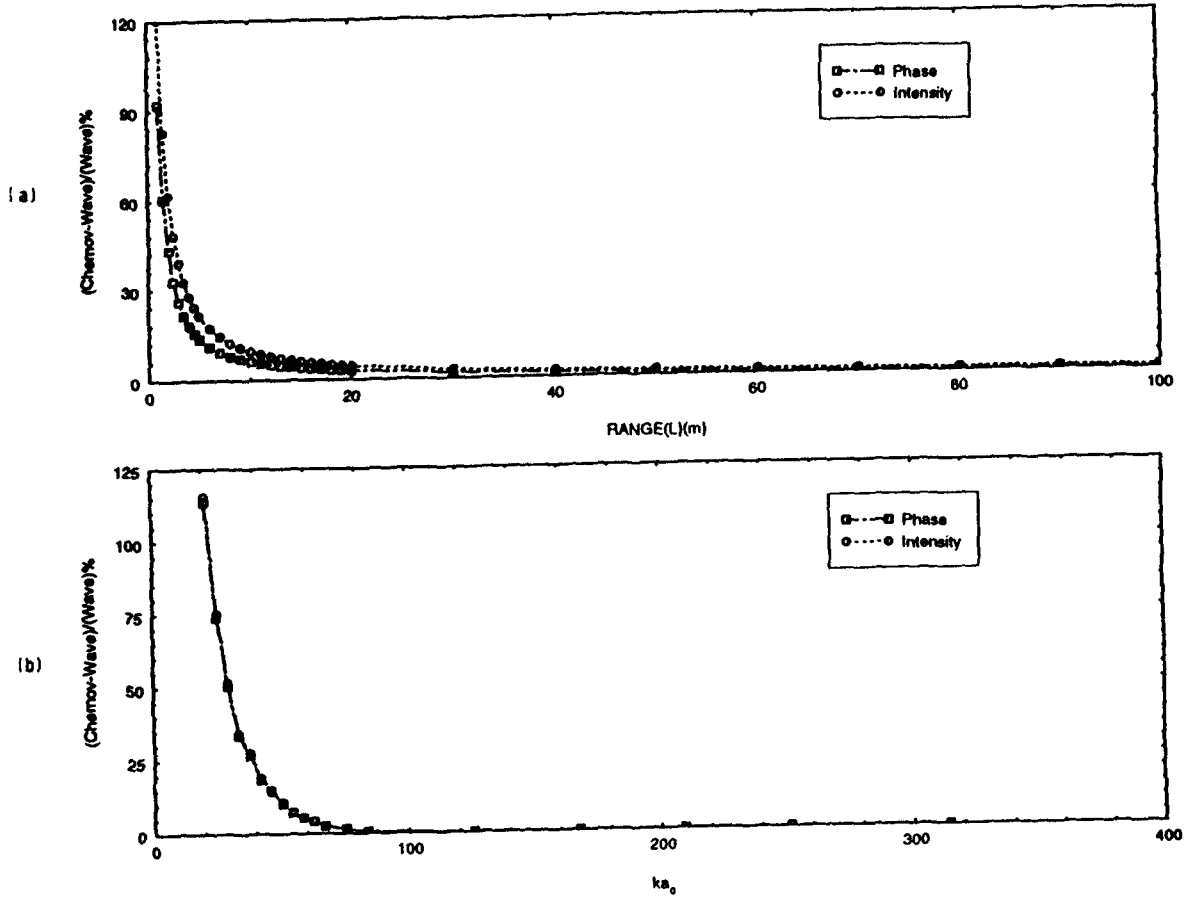

Figure 9: Comparison of rms relative intensity, and rms phase obtained from wave model, eqns. (14-17) with that of the Chernov model, eqns. (18,19) (a) as a function of the range L. $f = 100$ kHz, $a_0 = 2$ m, $\overline{\mu^2} = 5.1 \times 10^{-10}$, $ka_0 = 837.7$. (b) as a function of ka_0. $f = 100$ kHz, $\overline{\mu^2} = 5.1 \times 10^{-10}$ max $(a_0) = 0.75$.

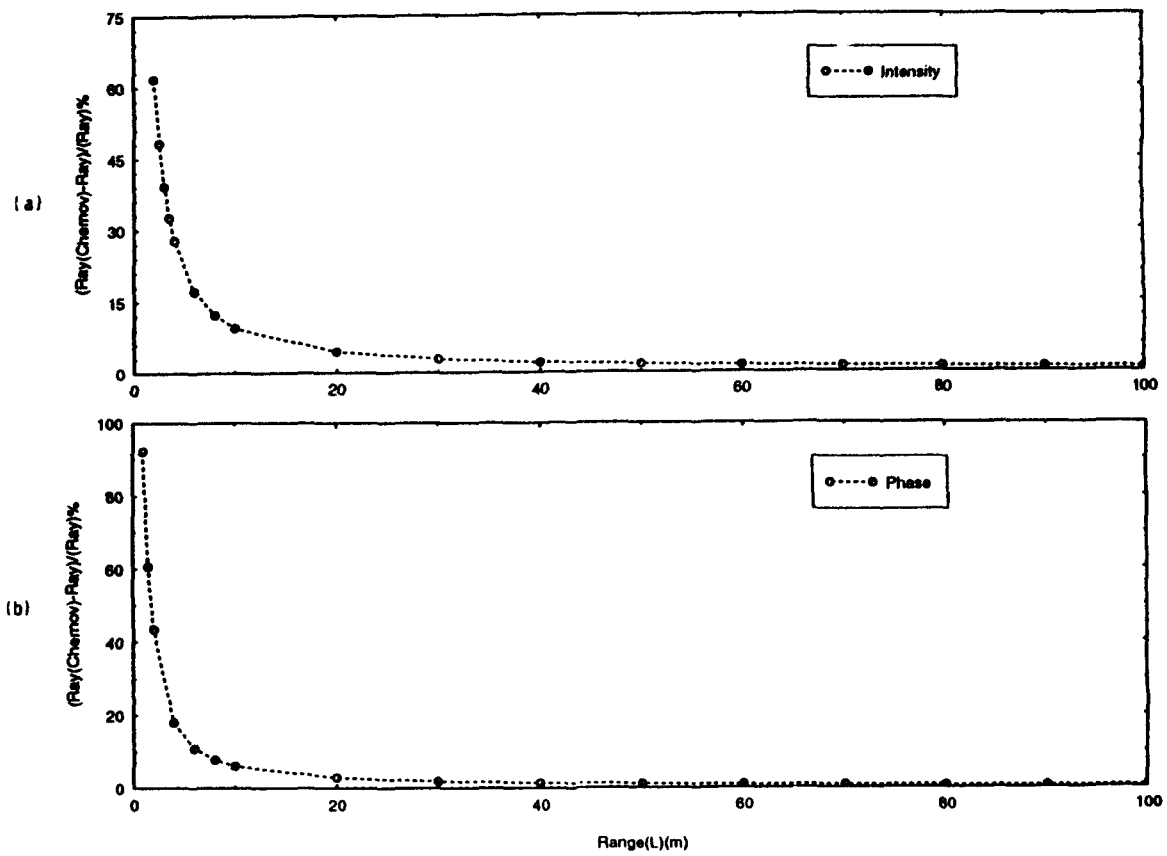

Figure 10: *Comparison of the (a) rms relative intensity and (b) rms phase obtained from the ray model, eqns. (23, 22) with that of the Chernov ray model, eqns. (25,24) as a function of the range L.* $f = 200$ kHz, $\overline{\mu^2} = 5.1 \times 10^{-10}$, $a_0 = 2$ m, $ka_0 = 1676$.

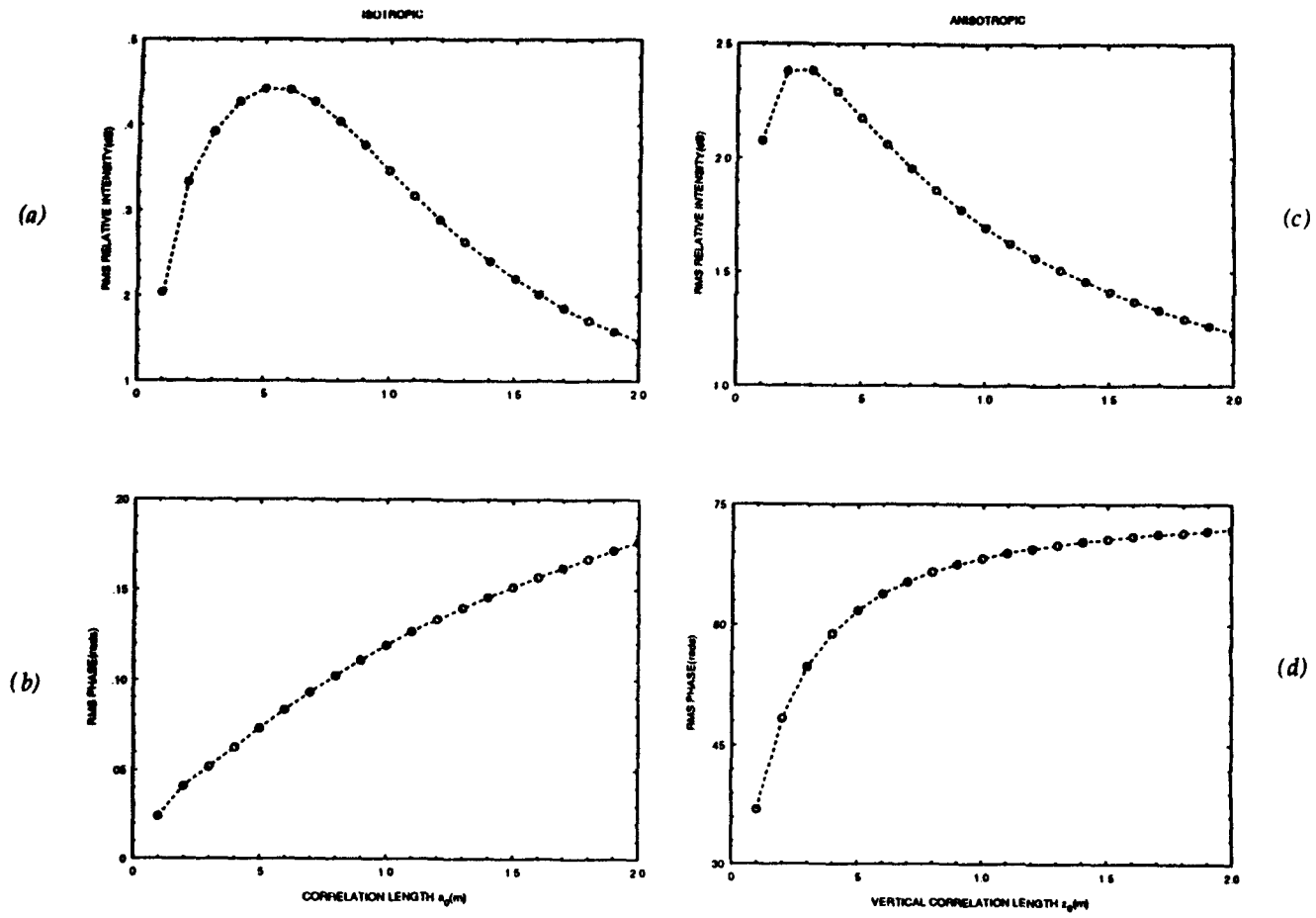

Figure 11: *RMS relative intensity (dB) and rms phase (radians) as a function of the correlation length for the isotropic (a, b) and anisotropic (c, d) media.* $L = 100$ *m,* $\overline{\mu^2} = 5.1 \times 10^{-10}$, $f = 100$ *kHz. For the anisotropic medium* $\rho_0 = 50$ *m. Used eqns. (14-17), for the isotropic medium and eqns. (14, 15, 27-30) for the anisotropic medium.*

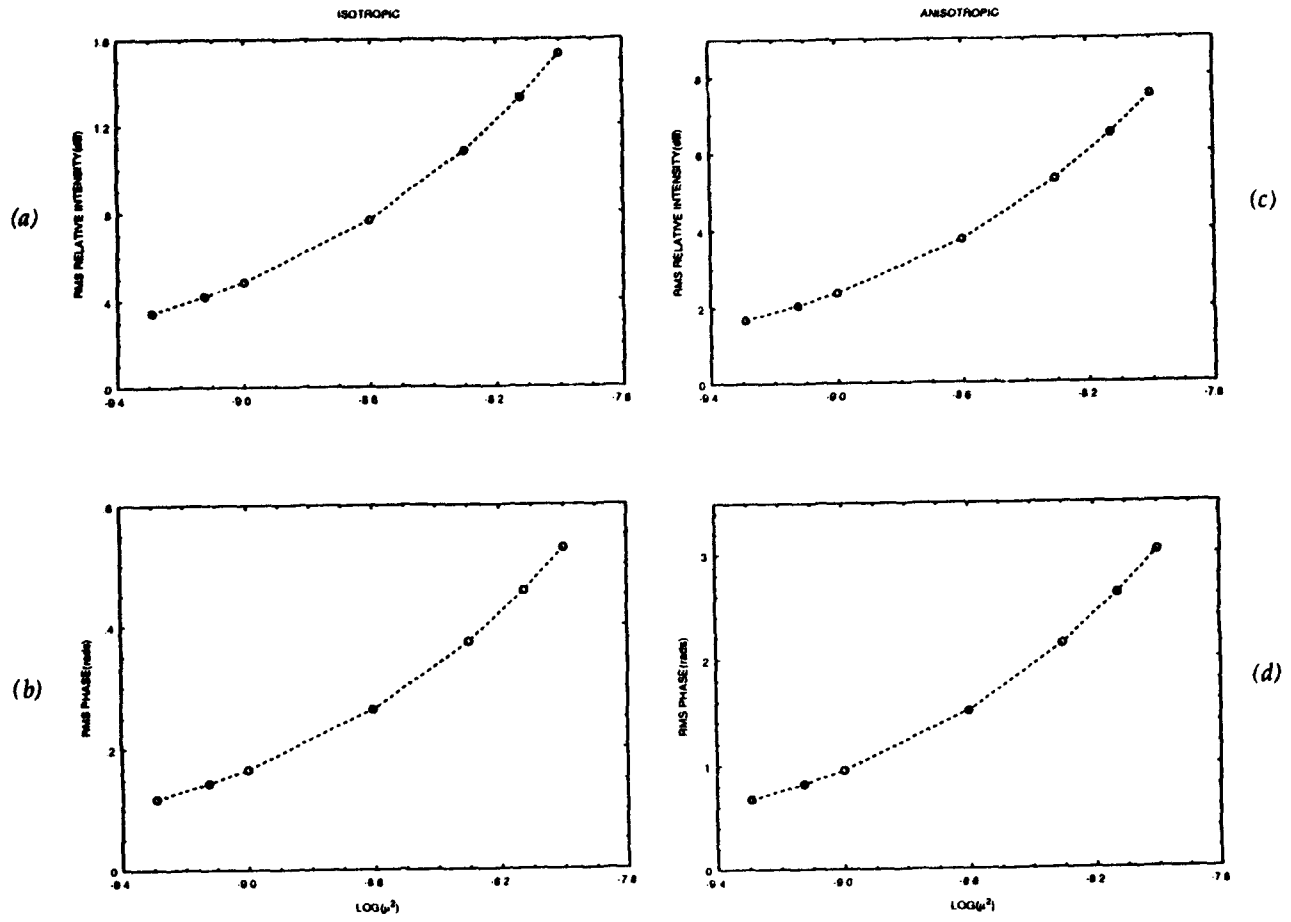

Figure 12: *RMS relative intensity (dB) and rms phase (radians) as a function of* $\overline{\mu^2}$*, for the isotropic (a, b) and anisotropic (c, d) media.* $L = 100$ *m,* $f = 100$ *kHz. For the isotropic media,* $a_0 = 1.0$ *m, and for the anisotropic media* $z_0 = 1$ *m,* $\rho_0 = 50$ *m. Used eqns (14-17), for the isotropic medium and eqns. (14, 15, 27-30) for the anisotropic medium.*

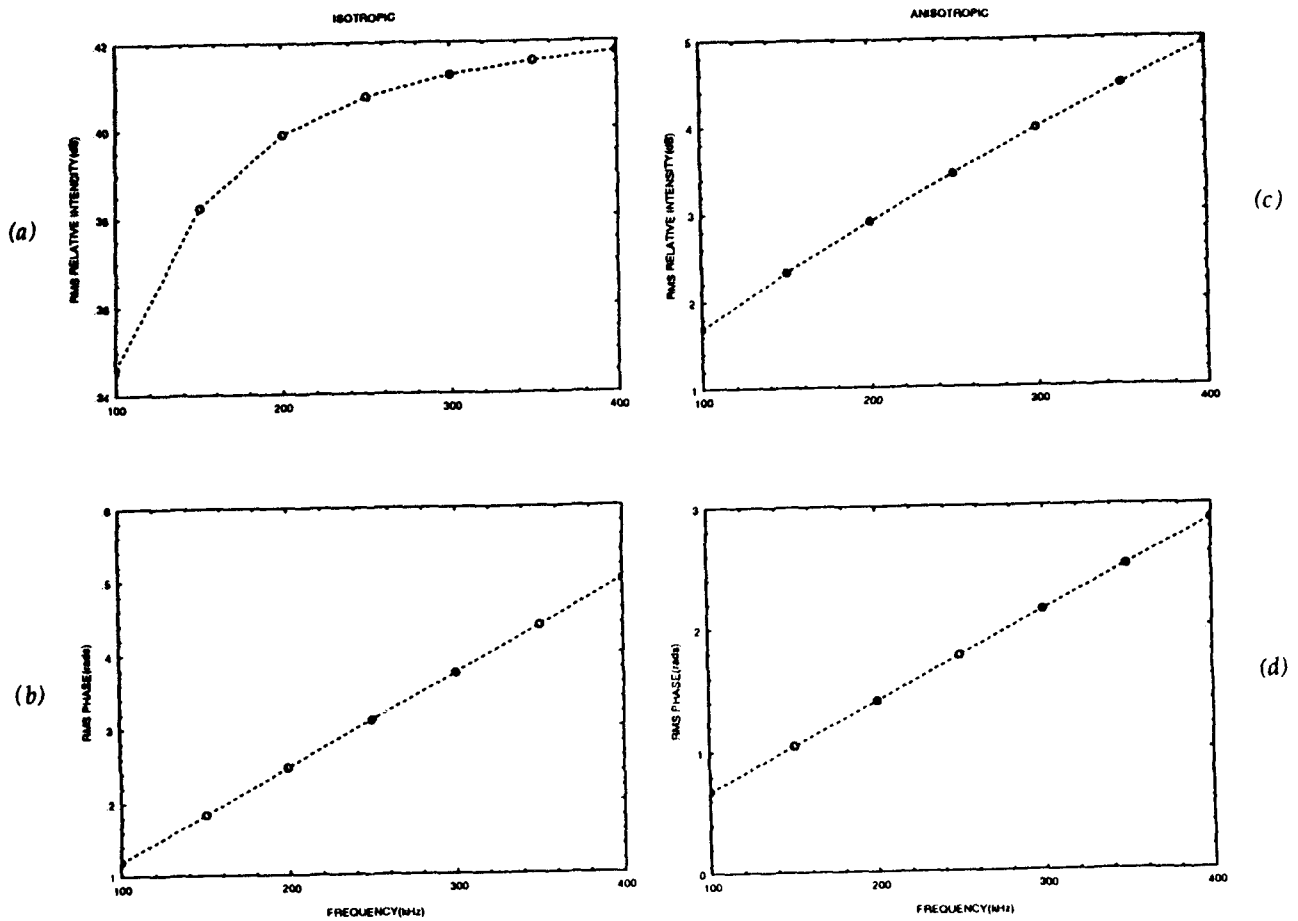

Figure 13: *RMS relative intensity (dB) and rms phase (radians) as a function of frequency for the isotropic (a, b) and anisotropic (c, d) media.* $\overline{\mu^2} = 5.1 \times 10^{-10}$, $L = 100$ *m. For the isotropic media,* $a_0 = 1.0$ *m, and for the anisotropic media* $z_0 = 1$ *m,* $\rho_0 = 50$ *m. Used eqns. (14-17), for the isotropic medium and eqns. (14, 15, 27-30) for the anisotropic medium.*

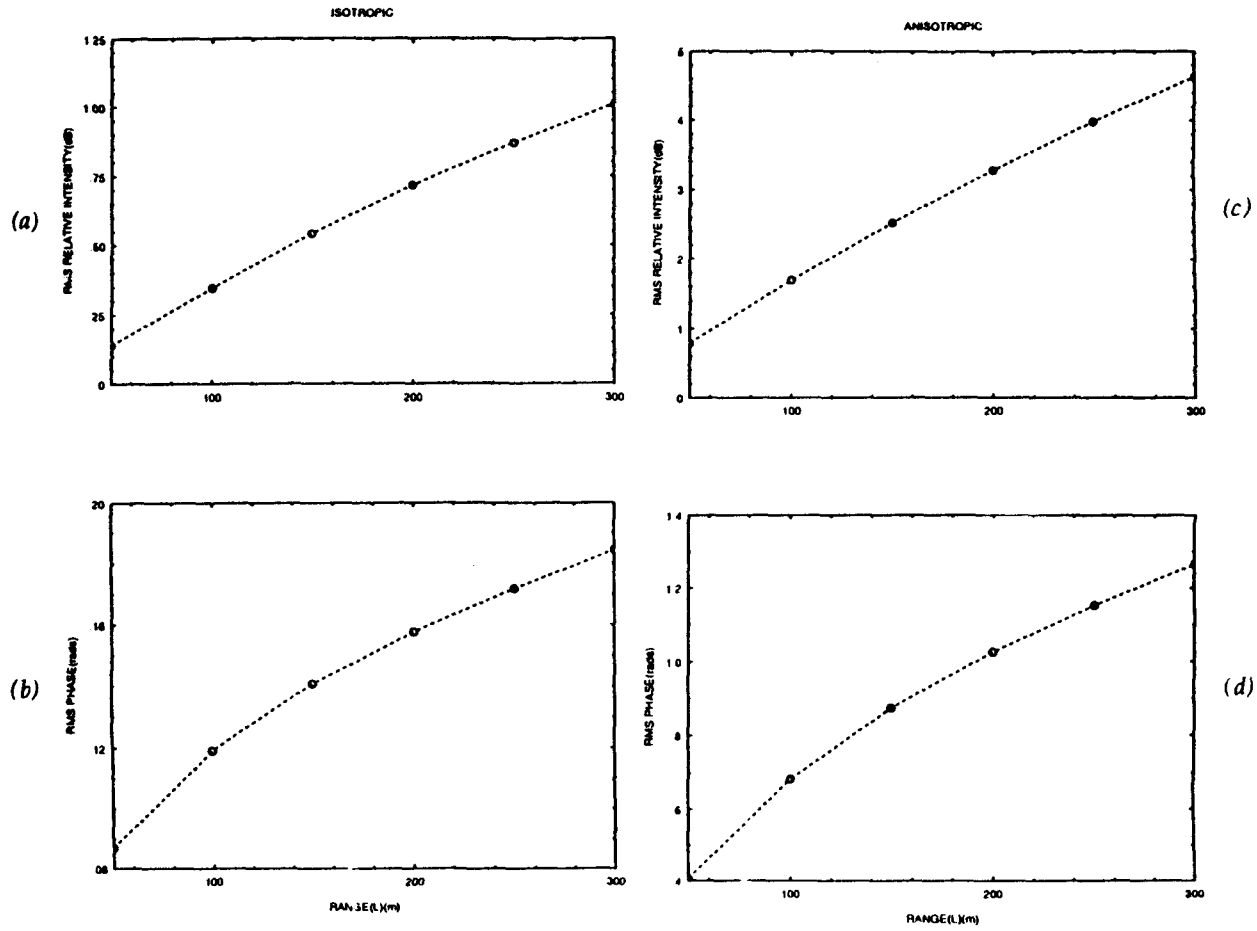

Figure 14: *RMS relative intensity (dB) and rms phase (radians) as a function of the range (L) for the isotropic (a, b) and anisotropic (c, d) media.* $\overline{\mu^2} = 5.1 \times 10^{-10}$, $f = 100$ *kHz. For the isotropic media,* $a_0 = 1.0$ *m, and for the anisotropic media* $z_0 = 1$ *m,* $\rho_0 = 50$ *m. Used eqns. (14-17), for the isotropic medium and eqns. (14, 15, 27-30) for the anisotropic medium.*

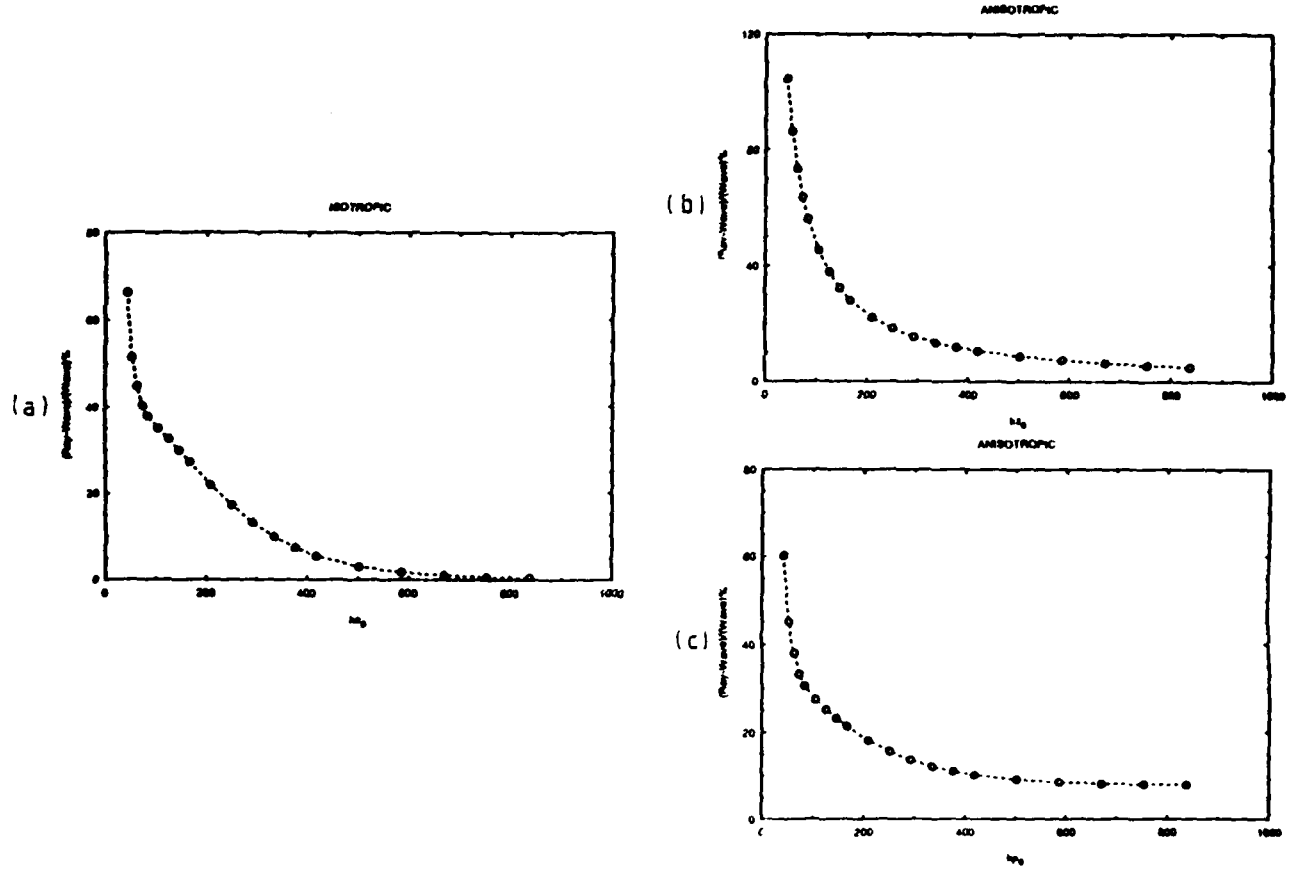

Figure 15: *Comparison of the rms phase obtained from the stochastic wave model, with that of the ray model, eqn (22) (a) as a function of ka_0, (b) as a function of kz_0, (c) as a function of $k\rho_0$ at two different frequencies 100 kHz and 300 kHz. L = 100 m, $\overline{\mu^2} = 5.1 \times 10^{-10}$. For (b), ρ_0 = 50 m and for (c) z_0 = 1 m. Used eqns (15-17) for the isotropic medium and eqns (15, 27, 30) for the anisotropic medium. a_0, is the isotropic correlation length, z_0, ρ_0 the anisotropic vertical and radial correlation lengths. k is the wave number*

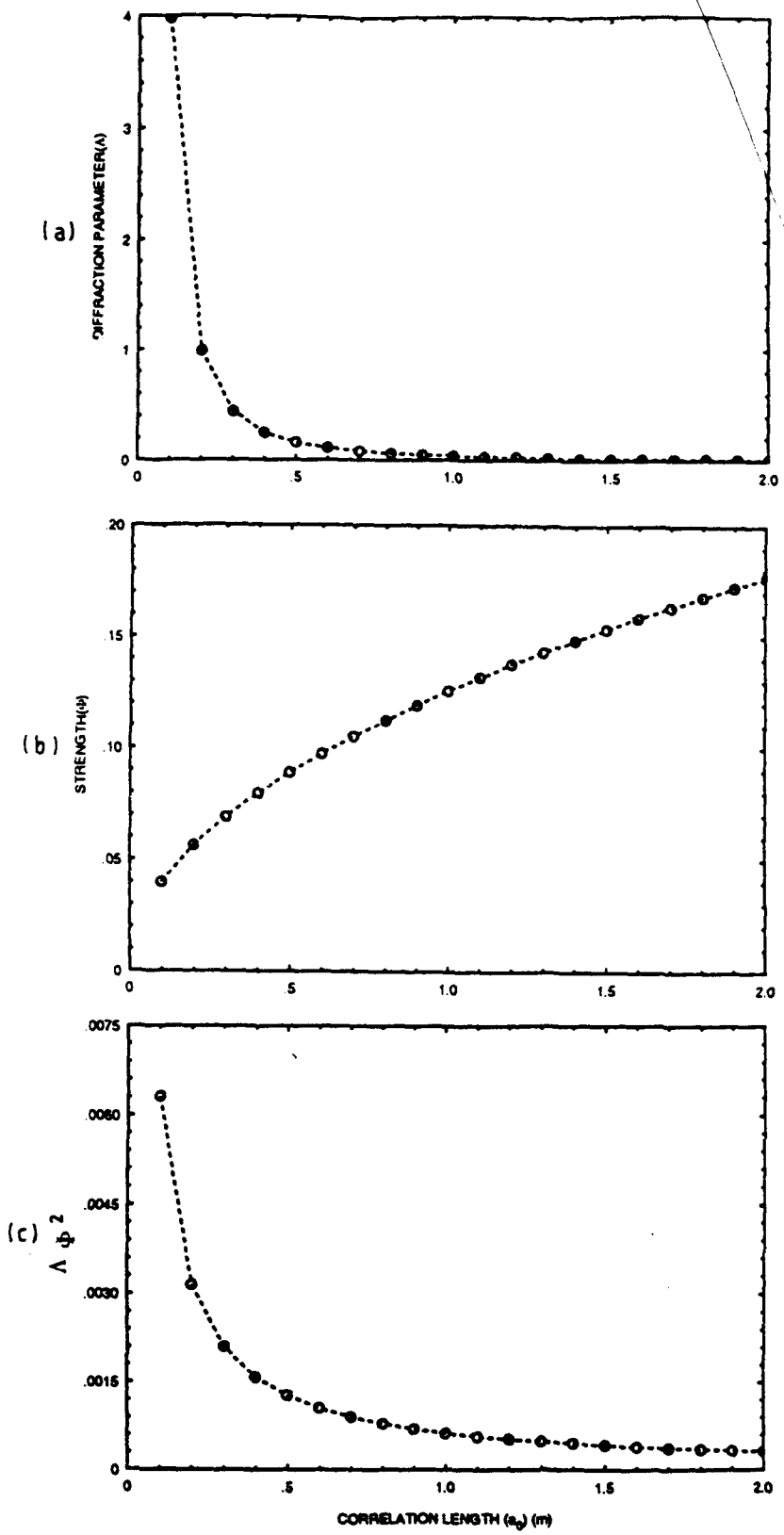

Figure 16: *(a) Plot of* Λ *(eqn (31)), (b) Plot of* Φ *(eqn (22)), (c) Plot of* $\Lambda\overline{\Phi^2}$ *as a function of the isotropic correlation length* a_0. $f = 100$ *kHz,* $L = 100$ *m,* $\overline{\mu^2} = 5.1 \times 10^{-10}$.

4.4 *Numerical Estimates of Intensity and Phase Fluctuations for the Anisotropic Correlation Function in the Wave and Ray Models*

This section gives some numerical estimates of high frequency intensity and phase fluctuations using the anisotropic correlation function. The variation with the radial and vertical correlation lengths, range, $\overline{\mu^2}$, and frequency are examined. In addition, the wave model results are compared with the results of the stochastic ray model.

Figures 11(c) and Fig. 11(d) show the rms relative intensity fluctuations (eqns (14, 27-30)), and rms phase fluctuations (eqns (15, 27-30)), for different values of the vertical correlation length z_0. As for the isotropic case, the NAG routines D01AJF and D01GAF are used to evaluates the integrals I_1 and I_2 (eqns (27) and (28)). Using an interval of $5X10^{-3}$ for the outer integral, a relative error of less than 1% is achieved in the double integral. The NAG routines S20ADF and S20ACF evaluate the Fresnel integrals $S(q)$ and $C(q)$ (eqn (30)) respectively. The correlation length z_0 varies from 10 cm to 2 m. The values of the other parameters used are $L = 100$ m, $\rho_0 = 50$ m, $\overline{\mu^2} = 5.1X10^{-10}$, and $f = 100$ kHz. The results using the anisotropic correlation function are in general similar to that obtained using the isotropic correlation function, except that the variations are much higher. The variation in the relative intensity is around 1.25 dB compared to about 0.3 dB for the isotropic case. For the phase fluctuations the variations are about 0.4 radians as compared to 0.15 radians for the isotropic case. This increase could be due to increased scattering at angles close to the direction of propagation, as a result of the anisotropy.

Figures 17(a) and (b) show the rms relative intensity (eqns(14, 27-30)), and phase fluctuations (eqns (15, 27-30)), for different values of the radial correlation distance ρ_0. The radial correlation distance varies from 10 cm to 100 m. The values of the other parameters used are $z_0 = 1$ m, $\overline{\mu^2} = 5.1X10^{-10}$, $f = 100$ kHz, and $L = 100$ m. The relative intensity variations and phase variations are approximately 1.5 dB and 0.8 radians respectively.

Figures 12(c) and (d) show the rms relative intensity and phase fluctuations for different values of $\overline{\mu^2}$. The variation in $\overline{\mu^2}$ corresponds to a temperature fluctuation that varies from $7X10^{-3}$ to $3X10^{-2}$ C degree at a particular depth and salinity. The values of the other parameters used are $f = 100$ kHz, $L = 100$ m, $z_0 = 0.7$ m, and $\rho_0 = 50$ m. The variation in acoustic fluctuation is much higher than that obtained with the isotropic correlation function. The variation in the rms relative intensity is about 6 dB, and the variation in phase is about 2.4 radians, over the range of $\overline{\mu^2}$ used. This shows that the rms intensity and phase fluctuations are sensitive to $\overline{\mu^2}$. The plot shown is a semi-logarithmic plot due to the range involved in $\overline{\mu^2}$. However a plot of the acoustic fluctuations against $(\overline{\mu^2})^{0.5}$ on a linear scale gives a straight line that passes through the origin.

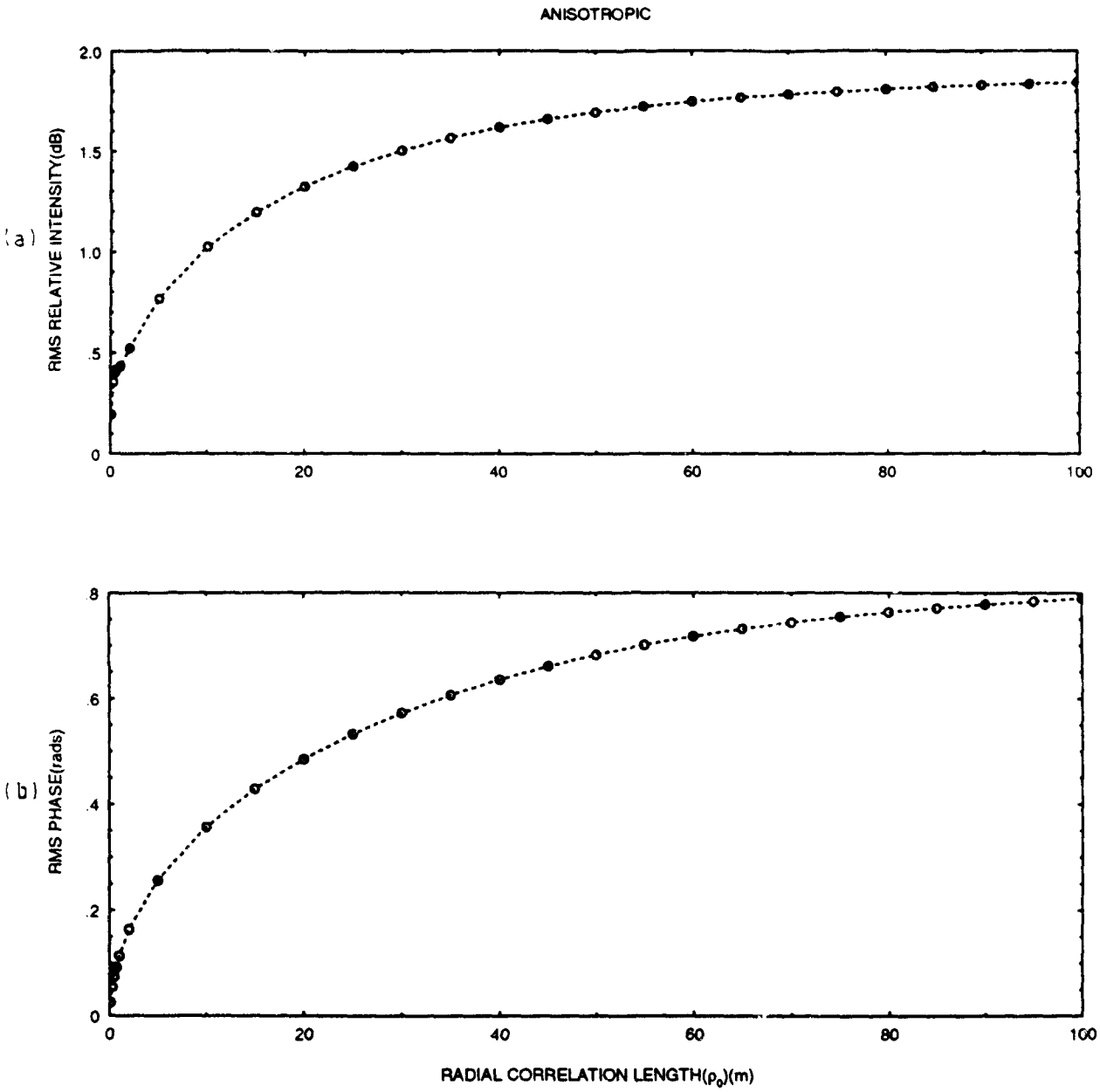

Figure 17: *(a) RMS relative intensity, eqns (14, 27-30) (b) and rms phase eqns (15, 27-30) as a function of the radial correlation length* ρ_0 *of the anisotropic medium,* $f = 100$ *kHz,* $L = 100$ *m,* $\overline{\mu^2} = 5.1 \times 10^{-10}$*, and* $z_0 = 1$ *m.*

Figures 13(c) and (d) show the variation of rms relative intensity and phase fluctuations as a function of frequency, where the frequency varies from 100 kHz to 400 kHz. The values of the other parameters used are $\overline{\mu^2} = 5.1X10^{-10}$, $L = 100$ m, $\rho_0 = 50$ m and $z_0 = 0.7$ m. The rms relative intensity shows a near linear variation. The rms phase fluctuation increases linearly with frequency, as predicted by eqn (22). The result is similar to that obtained for the isotropic case. Agreement with the ray result is obtained at a lower frequency for the rms phase, than for the relative intensity. Comparison of the results for the two media indicates that for the anisotropic medium the rms phase is about 6 times larger and the relative intensity about 5-12 times larger than the isotropic medium, for the parameters chosen in this example.

Figures 14(c) and(d) show the variation of rms relative intensity and phase fluctuations as functions of range, where the range varies from 50 m to 300 m. The values of the other parameters used are $\overline{\mu^2} = 5.1X10^{-10}$, $z_0 = 0.7$ m, $\rho_0 = 50$ m and $f = 100$ kHz. The rms relative intensity shows a near linear relationship with range, with values on the average approximately 5 times larger than for the isotropic case. The rms phase variation shows a non linearity of $L^{0.6}$ initially, close to that predicted by the ray result (eqn (22, 24)). As the range increases, the variation becomes linear showing that for a particular frequency, the shorter the range, closer the agreement with the ray result. This is understood on the basis of the parameters Λ and Φ^2 introduced for the isotropic case, both of which increase with range. The rms phase values are higher by 5-7 times the value of the isotropic case, for the parameters used in this example.

Figures 15(b) and (c) compares rms phase fluctuations obtained from the wave model (eqns (14, 27-30)), with that of the stochastic ray model (eqn (22), with ρ_0 replacing a_0). This is shown in Fig. 15(b) as a function of $k_0 z_0$ and in Fig. 15(c) as a function of $k_0\rho_0$. The values of the other parameters used are $\overline{\mu^2} = 5.1X10^{-10}$, $L = 100$ m, and $f = 100$ kHz. In Fig. 15(b), $\rho_0 = 50$ m, and in Fig. 15(c), $z_0 = 1$ m. In both cases, the graphs indicate that agreement with the ray model improves with increase in $k_0 z_0$ and $k_0\rho_0$. Since the ray model results are obtained by making $k_0 a_0, k_0\rho_0 \rightarrow \infty$, the results follow the expected trends.

5. *Phase Structure Function using Stochastic Ray Theory*

In the previous sections we obtained estimates of the variance of the relative intensity and phase fluctuations at a point in space. On comparing the results of phase fluctuations obtained from the wave and ray models, it can be seen that for $L = 100$ m, if $k_0 a_0 > 500$, the difference between the models is less than 5%. This can be seen from Fig. 15(a). To obtain the same agreement in the anisotropic medium, $k_0 z_0$ and $k_0\rho_0$ must be greater than 600, as can be seen from Figs. 15(b) and (c). In high frequency mine imaging, the range involved is a few metres and frequencies are in the mega hertz band. To examine the accuracy of the stochastic ray model to predict the rms phase fluctuations under these conditions, wave model calculations (eqns (15-17) for the isotropic medium and eqns (15, 27-30) for the anisotropic medium), and ray model calculations (eqn (22)) are carried out with $\overline{\mu^2} = 5.1X10^{-10}$, $f = 1$ MHz, and $L = 3$ m. The results of these calculations

are shown in Fig. 18(a) as a function of the isotropic correlation length a_0, and in Fig. 18(b) as a function of the anisotropic correlation length ρ_0. In Fig. 18(b) $z_0 = 2$ m. The curves in Fig. 18 indicate that for $f = 1$ MHz, and $L = 3$ m the results of the two models are indistinguishable graphically. This shows that for these situations the stochastic ray model can provide good estimates of the variance of the phase fluctuations. This being the case, one may proceed to obtain estimates of the phase structure function in the ray approximation.

The phase structure function (PSF) is defined by [Flatte et al 1979, p108]

$$PSF(x) = \overline{[(\phi(R_1) - \overline{\phi(R_1)}) - (\phi(R_2) - \overline{\phi(R_2)})]^2} \tag{32}$$

where $\phi(R_1), \phi(R_2)$ are the phases of the signal at receivers R_1, R_2, $\overline{\phi(R_1)}, \overline{\phi(R_2)}$ their mean values, and x the distance of separation between the receivers. The phase structure function gives the variance of the phase difference between two points caused by sound speed fluctuation. Expanding *PSF(x)*, it can be written as

$$PSF(x) = \overline{(\Delta\phi(R_1))^2} + \overline{(\Delta\phi(R_2))^2} - 2\overline{\Delta\phi(R_1)\Delta\phi(R_2)} \tag{33}$$

where $\Delta\phi(R) = \phi(R) - \overline{\phi(R)}$. In eqn(33) $\overline{(\Delta\phi(R_1))^2}$ is the variance of the phase fluctuation at receiver 1 and $\overline{(\Delta\phi(R_2))^2}$ is the variance of the phase fluctuation at receiver 2. The term $\overline{\Delta\phi(R_1)\Delta\phi(R_2)}$ is the spatial auto correlation function of the phase fluctuations. The phase structure function therefore involves the variances of the phase fluctuation at receivers 1 and 2 and the spatial auto correlation function of the phase fluctuations. If the variance of the phase difference between the two receivers is large then the coherence between the two signals is small and vice versa, [Esswein and Flatte, 1981]. Since the phase structure function is a measure of variance of the phase difference at the two receivers, it is a useful parameter in the evaluation of coherence. The phase structure function is also seen as a measure of correlation between the signals at the two receivers. If the signals are completely independent then PSF(x) approaches a value that is the sum of the variance of the phase fluctuations at the two receivers.

Let us now estimate the phase structure function due to thermal fluctuations in the ray approximation. Suppose we have the source at (0, 0, 0), receiver R_1 at $(R,0,0)$ and R_2 at $(X_2,0,z)$, where $X_2^2 + z^2 = R^2$. That is both receivers are at the same distance from the source but are in different directions, one being at a different depth. Using the expression for *PSF* in terms of the correlation function, [Esswein and Flatte, 1981] and sustituting the isotropic correlation function [eqn 7(a)], one obtains

$$PSF(z) = k_0^2 \overline{\mu^2} \sqrt{\pi} a_0 [2R\, erf(R/a_0) + 2\frac{a_0}{\sqrt{\pi}}(e^{-R^2/a_0^2} - 1) - P_{11}] \tag{34}$$

where

$$P_{11} = R\int_0^1 dx\; e^{-z^2x^2/a_0^2}[erf(\frac{R - X_2x}{a_0}) + erf(\frac{X_2x}{a_0})]. \tag{35}$$

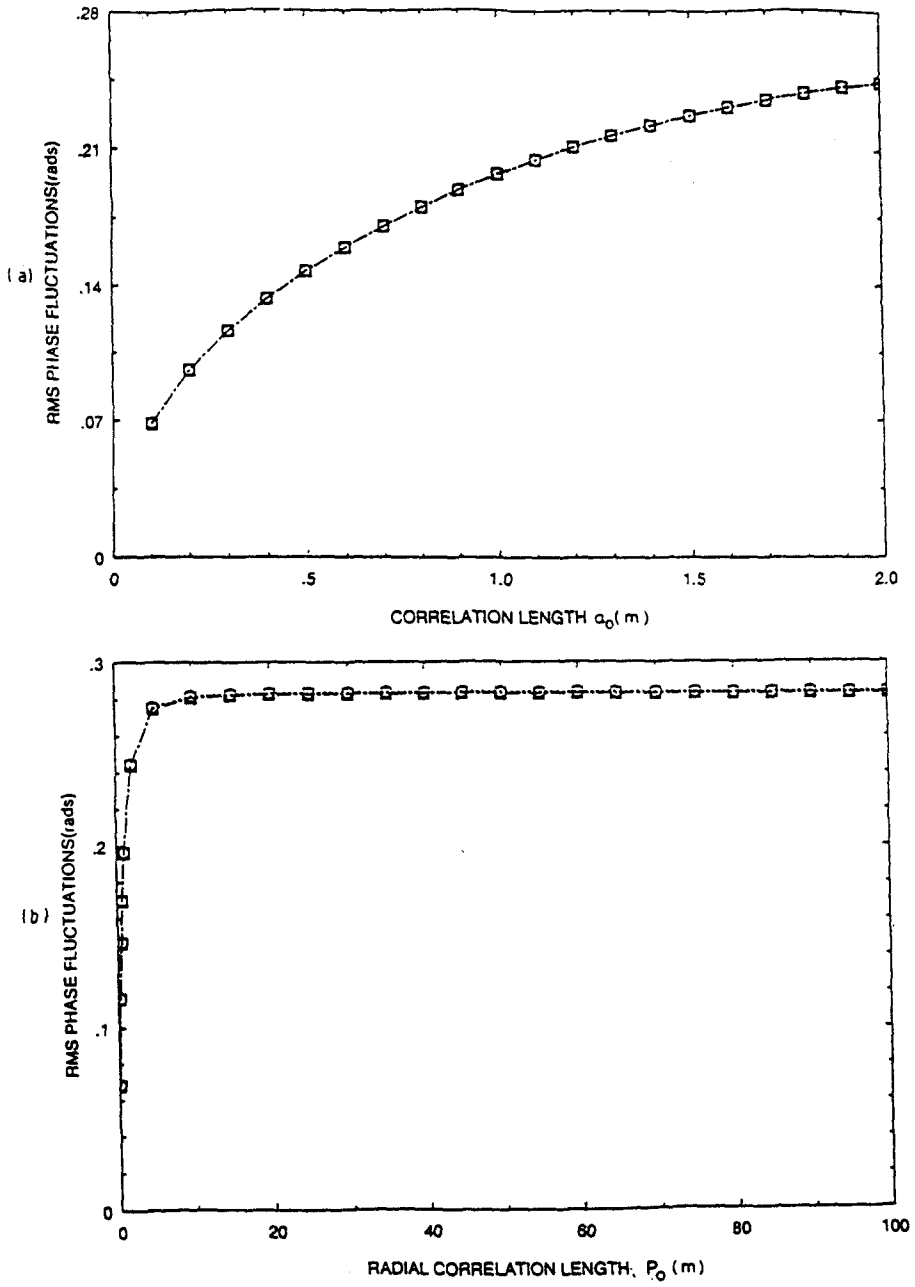

Figure 18: *Comparison of the RMS phase fluctuations from the wave model, for an isotropic (eqns 15-17) and anisotropic (eqns 15, 27-30) medium, with the stochastic ray model, eqn (22).* $f = 1$ *MHz,* $L = 3$ *m and* $\overline{\mu^2} = 5.1 \times 10^{-10}$. *(a) as a function of* a_0, *the isotropic correlation length. (b) as a function of* ρ_0, *the anisotropic radial correlation length, with the vertical correlation length* $z_0 = 2$ *m. The 2 curves are indistinguishable within graphical accuracy.*

For the anisotropic correlation function [eqn (7b)],

$$PSF(z) = k^2\overline{\mu^2}\rho_0[\sqrt{\pi}R\, erf(R/\rho_0) + \rho_0(e^{-R^2/\rho_0^2} - 1) + P_{22} - P_{33}] \quad (36)$$

where

$$P_{22} = (1+m^2)[2(b\rho_0 + X_2)\int_b^{b+X_2/\rho_0} e^{-(t^2-b^2)}dt + \rho_0(e^{-X_2^2/\rho_0^2 - 2bX_2/\rho_0} - 1)] \quad (37)$$

$$P_{33} = R\sqrt{\pi}\int_0^1 dx\; e^{-|z|x/z_0}[erf(\frac{R - X_2x}{\rho_0}) + erf(\frac{RX_2}{\rho_0})] \quad (38)$$

in which $b = |m|\rho_0/2z_0$, $|m| = |z|/X_2$. The above expressions for the phase structure function are obtained assuming the path of the ray between the source and receiver to be a straight line. This is a reasonable assumption for a range of a few metres and when the mean gradient is small. There is no restriction on the separation between receivers.

When the two rays are almost parallel to the X axis, with the receiver R_2 positioned at *(R, 0, z)*, for the isotropic correlation function,

$$PSF(z) = 2\Phi_1^2(1 - e^{-z^2/a_0^2}) \quad (39)$$

and for the anisotropic correlation function,

$$PSF(z) = 2\Phi_1^2(1 - e^{-z/z_0}) \quad (40)$$

where Φ_1^2 is the mean square phase fluctuation at R_1, $\Phi_1^2 = \overline{(\Delta\phi(R_1))^2}$, given by eqn (22). For the anisotropic function ρ_0 replace a_0 in eqn (22). The assumption that two rays are parallel would be a reasonable approximation at large range and for small separation between the receivers. One can also derive eqn(39) in the ray approximation for an isotropic medium using $R >> a_0$, $z \approx a_0$, and the spatial auto correlation coefficient of the phase fluctuations obtained by Chernov [1960, p107]. This indicates that the closed form eqns (39) and (40) are valid only at large range and for small separation between the receivers. No expressions are given by Chernov for small R or for the anisotropic case.

Let us now examine the results of some numerical simulations carried out for the PSF. Consider first the isotropic medium. Fig. 19(a) is a plot of $PSF(z)/\Phi_1^2$ (eqns (34, 35, 22)) as a function z/R, where R is equal to 3 m. The two plots correspond to a_0 =1 and 2 m. The expression $PSF(z)/\Phi_1^2$ is independent of $\overline{\mu^2}$ and frequency, and depends only on R, a_0 and z. This can easily be seen from eqns (34, 35, 22). Since R is comparable to a_0, use of eqn (39) to obtain $PSF(z)/\Phi_1^2$ would be inappropriate. The integral that occurs in eqn (35) is evaluated numerically using the NAG routine D01AJF. A relative error of less than 1% in the integral is obtained by specifying the relative error in the routine to be less than

10^{-4}. A qualitative understanding of the variation with a_0 is obtained using eqn (39). This indicates that for small a_0, the value of z to reach saturation is also small.

Figure19(b) shows the plot of $PSF(z)/\Phi_1^2$ as a function of z/a_0 where $a_0 = 0.1$ m and $R = 3$ m. PSF(z) is calculated using eqns (39, 22) as well as eqns (34, 35). For $R >> a_0$, eqn (39) would be appropriate only at short separations. The calculations are carried out with receiver R_2 being positioned at $(R, 0, z)$. At small separations, where $z < 0.5a_0$, the results of both approximations agree. However, at large z, discrepancies appear, where the parallel approximation ((eqn.(39)) fails. At very large vertical separations, both approximations give a value of 2 for $PSF(z)/\Phi_1^2$. This is true always for an isotropic medium and cannot be used to distinguish between the approximations. For an isotropic medium the first two terms of the *PSF* given in eqn (34) are equal for all separations z, provided the distances between the source and receivers are the same. The third term decreases to zero at large separations. This accounts for the result observed at large vertical separations. Figures 19(a), (b) show that as a_0 decrease, the separation at which saturation occurs also decrease. As a_0 decreases, the distance over which the acoustic phase fluctuations are correlated decreases, which in turn causes the distance at which saturation occurs to decrease.

Let us now consider an anisotropic medium. In this case the phase fluctuations at positions that are separated from the source by the same distance *R* but are in different directions in the xz plane will not be the same. When the angle of inclination of the receiver measured from the horizontal direction increases, there is a decrease in the variance of the fluctuations at the receiver. This is because the temperature fluctuation decays much faster in the vertical direction than in the radial direction, resulting in a reduction in the acoustic fluctuation. For large separation we would therefore expect that a plot of $PSF(z)/\Phi_1^2$ as a function of z/R to approach 1. The parallel ray approximation (eqn.(40)) clearly fails at large z where it approaches a value of 2. This is because the two paths to the receivers are the same in the parallel ray approximation. Figure 20 is a plot of $PSF(z)/\Phi_1^2$ as a function of z/R. The calculations are carried out with $\rho_0 = 75$ m, $R = 3$, and $z_0 = 0.1, 0.5$ m. Since $R << \rho_0$, eqns (36,37,38,22) are used to evaluate the *PSF*. The integral that appears in eqns (37) and (38) is again evaluated numerically using the NAG routine D01AJF. A relative error of less than 1% for the integral is obtained by specifying the relative accuracy to be less than 10^{-4} in the routine. When z_0 is small, saturation is reached at small vertical separations. The results display the expected trends.

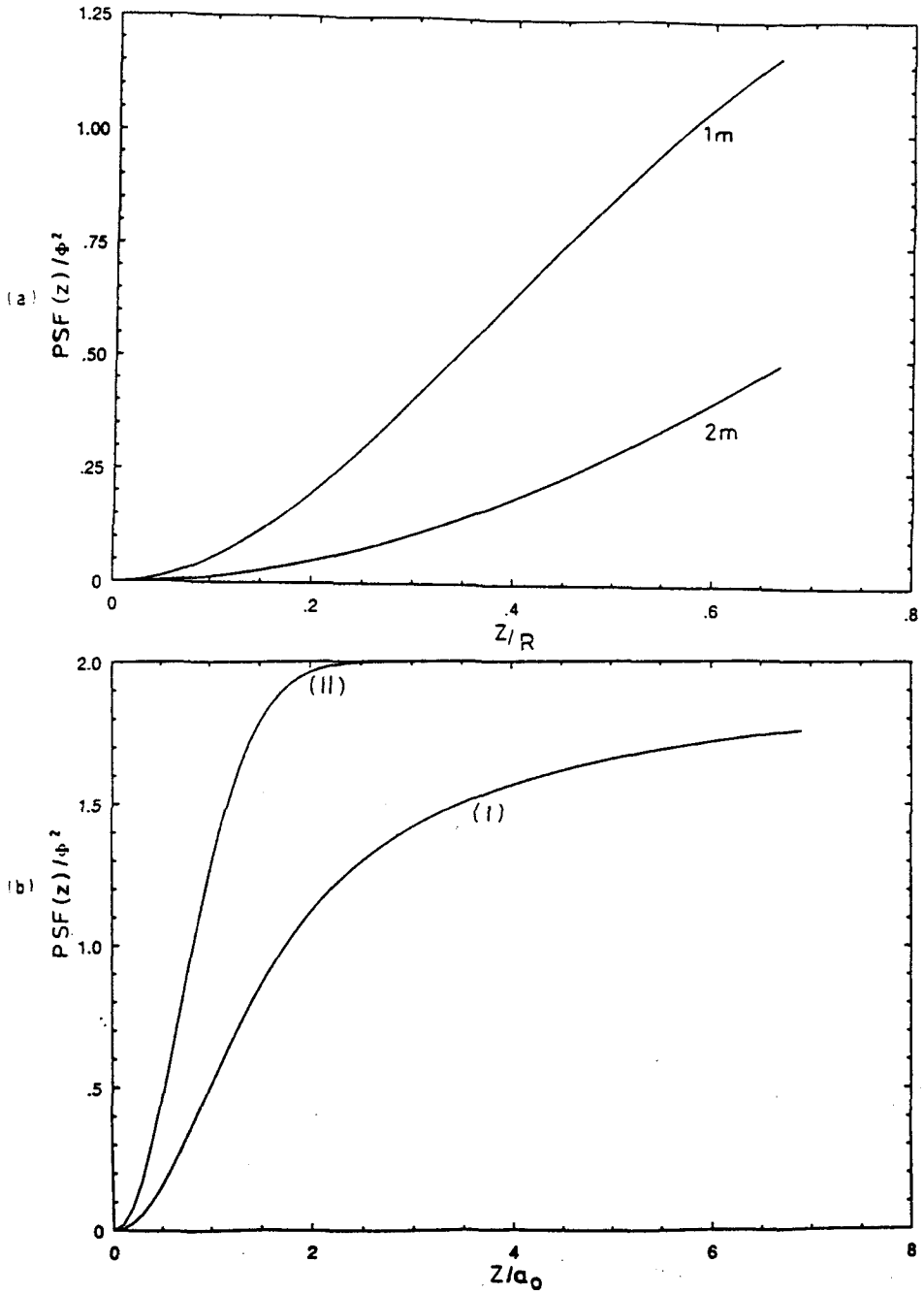

Figure 19: *Plots of ($PSF(z)/\Phi^2$) as a function of (a) z/R, (b) z/a_0 for an isotropic medium. z is the vertical separation between the 2 receivers, and Φ^2 the mean square phase fluctuation at receiver 1. R = 3 m. (a) Curve (1) is for a_0 = 2 m and curve (2) for a_0 = 1 m. Both curves plotted using eqns (22, 34, 35). (b) Curve (1) plotted using eqns (22, 34, 35) and curve (2) using eqn (39). In (b) both curves use a_0 = 0.1 m. Graph (b) compares the linear and parallel approximations.*

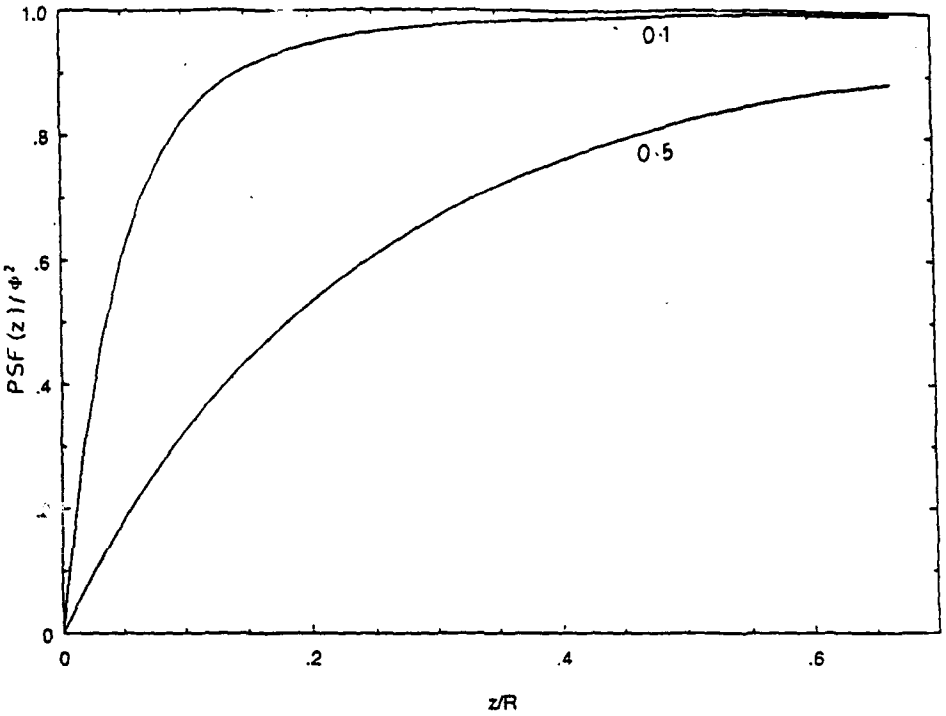

Figure 20: Plots of $(PSF(z)/\overline{\Phi_1^2})$ (eqns 22, 36-38) as a function of z/R for an anisotropic medium, $z_0 = 0.1$ and 0.5 m. $R = 3$ m, $\rho_0 = 75$ m.

6. Summary

In this paper suitable models to obtain high frequency acoustic scattering estimates due to temperature changes were examined. Previously models were restricted to long range, and did not treat the anisotropy of the fluctuations. There was thus a need to correct this problem. Other questions that were looked into include the validity of the stochastic ray model at high frequencies (say 100 kHz and above), theoretical estimates for the phase structure function, and estimates of intensity and phase changes due to the mean temperature gradient.

Section 2 shows some experimental temperature and temperature gradient profiles. They show the type of data obtained experimentally, and give a feeling for the magnitudes of the temporal and spatial variation of temperature. Near surface layers, there are temperature inversions, and the average temporal variation of temperature ranges from 10^{-2} to 10^{-1} C deg per min (Figs.(3, 4)). The temperature gradient is responsible for acoustic refraction. The average

temperature gradient in the vertical direction, obtained from the ocean data near Perth, shows a value of -0.1 C deg /m. However at some positions in the profile the temperature gradients are much higher, close to -0.15 C deg/m. The gamma probability distribution function [Hayes et al, 1975] fits quite well to the discrete probability function of the temperature gradient.

Section 3 gives results for intensity and phase changes due to the mean temperature gradient. Expressions for intensity changes, eqns (1, 3), and phase changes, eqns (5, 6), due to the mean temperature gradient are given. They were obtained from deterministic ray theory. The reference point in the evaluation of these changes is a medium where there is no temperature gradient. For vertical rays where Officer's eqn (2) is invalid, analysis of eqn (4) indicates no intensity or phase change. Equation (4) also fails at $\theta = \pi/2$ which corresponds to a turning point. Ray solutions always fail at turning points. Since the acoustic velocity must be positive, for θ_0 not equal to 0, the horizontal range L cannot be equal to 0. The expressions obtained, eqns (1, 3, 5, 6), enable one to obtain intensity and phase changes due to variations in the mean temperature gradient, in regions where the ray approximation is valid.

Section 4 and beyond discusses models to obtain acoustic estimates due to the random part of the temperature. Equation (8) is the expression for the scattered pressure, using a stochastic wave model. Numerical calculations of the angular distribution of the scattered pressure for high frequency sound (Figs.7, 8) both for anisotropic and isotropic media indicate scattering being confined to an angle close to the direction of propagation. For attenuation in an isotropic medium, an expression has been available for some time, eqn (12) [Chernov, 1960, p55]. In an anisotropic medium, attenuation depends on the direction of propagation. When the direction of propagation is along the Z axis, attenuation is given by eqn (13). At 1 MHz the attenuation is of the order of $5X10^{-2}$ dB/m. The magnitudes for the isotropic medium are of the same order. Attenuation varied as k_0^2 for frequencies above 100 kHz.

Section 4.2 examines analytically amplitude and phase fluctuations at a receiver separated by a horizontal range L from a continuous monochromatic acoustic source. The study is in the unsaturated region of the $\Lambda - \Phi$ space and uses stochastic wave and ray models. For an isotropic medium, with $k_0 a_0$ very much greater than 1 and range L very much greater than a_0, expressions (18) and (19) for acoustic fluctuations have been available in the wave model [Chernov, 1960, p83]. Equations (14-17) are the new results for acoustic fluctuations in an isotropic medium, valid at all ranges and frequencies. Numerical comparisons between the two models show (see Fig. 9) that the Chernov model is valid only for L very much greater than a_0, and $k_0 a_0$ very much greater than 1. Equations (14, 15, 27-30) give expressions for acoustic fluctuations in an anisotropic medium, which are valid at all ranges, and frequencies. The anisotropic case has not been treated previously.

Expressions (24) and (25) for acoustic fluctuations in the stochastic ray model have been available only for an isotropic medium and at large range, where L is very much greater than a_0 [Chernov, 1960, p29, 34]. Equations (22, 23) are the new results for the acoustic fluctuations in the ray approximation valid at all ranges for an isotropic medium. Numerical comparisons between the two ray models (Fig.10) show the Chernov model is valid only for L very much greater than a_0. Equation (22) with ρ_0 replacing a_0 gives the expression for the rms phase fluctuation in the stochastic ray model for an anisotropic medium. The anisotropic case has not been treated previously.

Sections 4.3 and 4.4 presents numerical estimates of intensity and phase fluctuations. Calculations at 100 kHz, with L equal to 100 m and a temperature fluctuation of $7 X 10^{-3}$ C deg, show the rms relative intensity fluctuations (dB) and rms phase(rads) for an anisotropic medium are on the average higher by a factor of 5-10, and 3-6 respectively, when compared with an isotropic medium, where the vertical correlation lengths are the same, and the radial correlation length is about 50 times larger. For these parameters the rms phase and the rms relative intensity for an isotropic medium are of the order of 0.1 radians and 0.3 dB respectively. The variation of the rms relative intensity and rms phase with $\overline{\mu^2}$, which is dependent on the magnitude of the temperature fluctuation, is linear both for the isotropic and anisotropic media. The variation of the acoustic fluctuations as a function of frequency for large $k_0 a_0$, obtained using the wave model, show that the agreement of the rms phase with the ray result occurs at a lower frequency than for the relative intensity. A shorter range gives better agreement with the ray model, since an increase in range increases the diffraction parameter and Φ^2. Comparison with the statistical ray model shows, that in the isotropic case diffraction effects become important at correlation lengths that are less than approximately $\sqrt{L/6k_0}$.

Finally, section 5 examines the evaluation of theoretical estimates for phase structure function, using the ray model. Agreement in the phase fluctuation estimates between the wave and ray models is within 5% for an isotropic medium with L equal to 100 m, if $k_0 a_0$ is greater than 500. The same agreement occurs in the anisotropic medium if $k_0 z_0$ and $k_0 \rho_0$ is greater than 600. At a range of 3 m and a frequency of 1 MHz, the results of the phase fluctuations from the two models show that they are indistinguishable graphically (Fig. 18). Equations (39) and (40) are the expressions of the phase structure function for an isotropic and anisotropic medium respectively, valid at ranges $L >> a_0, \rho_0$, and at separations $z \approx a_0, z_0$. In other words eqns (39), (40) are expressions for the phase structure function at large range and for small separations between receivers. One can also obtain eqn (39) in the ray approximation, using the spatial auto correlation function of the phase fluctuations [Chernov, 1960, p107]. Equations (34, 35) and eqns (36, 37) are the expressions for the PSF of isotropic and anisotropic media respectively, valid at short range, and at all separations between receivers. At short range, the limiting value of $PSF(z)/\Phi_1^2$ for large z is 1 for the anisotropic medium, and 2 for an isotropic medium. At large range where L is very much greater than ρ_0, both approach the limiting value of 2.

7. Acknowledgments

The author wishes to thank Dr. I. S. F. Jones for his assistance throughout the course of this work and for providing the Woronora dam temperature data. The author also expresses his thanks to Mr. L. J. Hamilton for providing the temperature data off Perth and to Dr. M. Hall, whose valuable comments and assistance substantially improved this report.

8. References

1. Anderson, N. R., and Zahuranec, B. J. (1977). *Oceanic sound scattering prediction*. New York: Plenum press.

2. Chernov, L. A. (1960). *Wave propagation in a random medium*. New York: McGraw Hill.

3. Esswein, R., and Flatte, S. M. (1981). Calculation of phase-structure function density from oceanic internal waves. *Journal of Acoustical Society of America*, 70, pp 1387-1396.

4. Flatte, S. M., Dashen, R., Munk, W. H., Watson, K. M., and Zachariasen, F. (1979). *Sound transmission through a fluctuating ocean*. Cambridge, U. K: Cambridge University press.

5. Hayes, S. P., Joyce, T. M., and Millard Jr, T. R. (1975). Measurement of vertical fine structure in the Sargasso sea. *Journal of Geophysical Research*, 80, pp 314-319.

6. Joyce, T. M., and Desaubies, Y. F., (1977). Discrimination between internal waves and temperature fine structure. *Journal of Physical Oceanography* 7, pp 22-32.

7. Kravtsov, Yu. A., and Orlov,Yu. I. (1990). *Geometrical optics of inhomogeneous media*. Berlin: Springer-Verlag.

8. Libermann, L. J., (1951). The effect of temperature inhomogeneities in the ocean on the propagation of sound. *Journal of Acoustical Society of America*, 23, pp 563-570.

9. Liu, K. C., (1991). Wave scattering in discrete random media by the discontinuous stochastic field method, 1: Basic method and general theory. *Journal of Sound and Vibration*, 147, pp 301-311.

10. Medwin, H., (1975). Speed of sound in water; A simple equation for realistic parameters. *Journal of Acoustical Society of America* 58, pp 1318-1319.

11. Officer, C. B., (1958). *Introduction to the theory of sound transmission*. New York: Mcgraw Hill.

12. Tolstoy, I., and Clay, C. S. (1966). *Ocean acoustics: theory and experiment in underwater sound*. New York: Mcgraw Hill.

13. Unni, S., and Kaufman, C. (1981). Acoustic fluctuations due to temperature fine structure of the ocean. *Journal of Acoustical Society of America*, 69, pp 676-680.

14. Urick, R. J., (1983). *Principles of underwater sound*. New York: Mcgraw Hill.

Appendix

List of Symbols

f	frequency
f_i	inertial frequency
f_N	Brunt Vaisala frequency
c	sound velocity
k	wave number = $\frac{2\pi f}{c}$
t	time
T	degree Centigrade
S	salinity in ppt
r	positional coordinate
z	depth in m
g	velocity gradient
$p = \frac{\sin\theta_0}{c_0}$	c_0 speed of sound near source; θ_0 ray angle at source
s	ray path
ΔI	Intensity loss
φ	phase
Φ	root mean square phase fluctuation in the ray approximation
γ	used in equation (6)
$\overline{p_s(r)^2}$	mean square scattered pressure
υ	different temperature profiles
λ_0	wavelength of sound
Λ	diffraction parameter
$\overline{\mu^2}$	mean square fractional sound speed fluctauation

A, A_0	amplitude of received, transmitted sound wave
$N_2(r-r')$	covariance
$N(r-r')$	correlation coefficient
$\vec{K} = \vec{k}_i - \vec{k}_s$; i,s	denote direction of incident and scattered sound
$F(K)$	Fourier transform of $N(r-r')$
$F_1(K)$	frequency and angular part of the mean scattered pressure
α	total attenuation in dB/m
z_0, ρ_0	vertical and radial correlation length
a_0	isotropic correlation length
$\overline{(\ln(A/A_0))^2}$	mean square relative log amplitude fluctuation
$\overline{(\Delta\phi)^2}$	mean square phase fluctuation
I_1, I_2	integrals that appear in fluctuation formulae
IA, IB, IC, ID	defined by equations (29) and (30)
$S(q), C(q)$	Fresnel sine and cosine integrals
E_0	energy emitted per unit time per unit solid angle
$PSF(x)$	phase structure function
P_{11}, P_{22}, P_{33}	defined by equations (35), (37) (38)

SECURITY CLASSIFICATION OF THIS PAGE **UNCLASSIFIED**

REPORT NO.	AR NO.	REPORT SECURITY CLASSIFICATION
DSTO-RR-0001	AR-008-638	Unclassified

TITLE

Models to estimate high frequency acoustic scattering due to thermal fine- and micro-structure of the ocean

AUTHOR(S)
R.A. Thuraisingham

CORPORATE AUTHOR
DSTO Aeronautical & Maritime Research Laboratory
GPO Box 4331
Melbourne Victoria 3001

REPORT DATE	TASK NO.	SPONSOR
June, 1994	NAV 92/256	Navy

FILE NO.	REFERENCES	PAGES
G6/4/8-4647	14	54

CLASSIFICATION/LIMITATION REVIEW DATE

CLASSIFICATION/RELEASE AUTHORITY
Chief, Maritime Operations Division

SECONDARY DISTRIBUTION

Approved for public release

ANNOUNCEMENT

Announcement of this report is unlimited

KEYWORDS

Phase structure function
Acoustic fluctuations
Temperature gradients
Acoustic scattering
Thermal fluctuations

ABSTRACT

Existing models to obtain intensity and phase changes of sound due to thermal fluctuations in the ocean, such as that developed by Chernov, are limited in their application. They are valid only for an isotropic medium and where the range is much greater than the correlation distance of the fluctuations. Extensions to short range and for an anisotropic medium are described here, both for the stochastic wave and ray models. Theoretical expressions obtained for acoustic fluctuations are easily evaluated. Numerical estimates are provided using stochastic wave and ray models for certain parameters of range, frequency and temperature variation, of interest in target strength measurements. These estimates indicate acoustic fluctuations for an anisotropic medium are always higher than for an isotropic media. For a range of 100 m, frequency of 100 kHz and temperature fluctuation of 7×10^{-3} C deg, the root mean square relative intensities and the root mean square phase fluctuations are on the average higher by a factor of 6, where the vertical correlation lengths are the same and the radial correlation length is about 50 times larger. Closed form expressions in the deterministic ray approximation are given to evaluate intensity and phase changes due to the mean temperature gradient. The validity of the deterministic ray theory results is discussed. Results from the stochastic wave and ray models are examined for the applicability of the stochastic ray model at high frequencies. At mega hertz frequencies and ranges of 1-3 metres, which are of interest in acoustic mine imaging, estimates of the phase fluctuations from the stochastic ray approximation and the wave model are indistinguishable. Theoretical expressions of the phase structure function are given in the ray approximation to provide estimates of the phase coherence between signals. These results can provide valuable comparisons with experimental results, when such measurements are carried out with frequencies in the mega hertz band and at ranges of 1-3 metres.

SECURITY CLASSIFICATION OF THIS PAGE
UNCLASSIFIED

Models to Estimate High Frequency Acoustic Scattering Due to Thermal Fine- and Micro-Structure of the Ocean

R.A. Thuraisingham

(DSTO-RR-0001)

DISTRIBUTION LIST

Director, AMRL	
Chief, Maritime Operations Division	
B.F. Wild	
R.A. Thuraisingham	4 copies
Library, AMRL Maribyrnong	
Chief Defence Scientist (for CDS, FASSP, ASSCM)	1 copy only
Director, ESRL	
Library, AMRL Fishermens Bend	
Head, Information Centre, Defence Intelligence Organisation	
OIC Technical Reports Centre, Defence Central Library	
Officer in Charge, Document Exchange Centre	8 copies
Air Force Scientific Adviser, Russell Offices	
Navy Scientific Adviser	
Scientific Adviser - Policy and Command	
DASD, APW2-1-OA2, Anzac Park West, Canberra ACT	
Senior Librarian, Main Library DSTOS	
Librarian, DSD, Kingston ACT	
Serials Section (M List), Deakin University Library, Deakin University, Geelong 3217	
NAPOC QWG Engineer NBCD c/- DENGRS-A, HQ Engineer Centre, Liverpool Military Area, NSW 2174	
ABCA, Russell Offices, Canberra ACT 2600	4 copies
Librarian, Australian Defence Force Academy	
Head of Staff, British Defence Research and Supply Staff (Australia)	
NASA Senior Scientific Representative in Australia	
INSPEC: Acquisitions Section Institution of Electrical Engineers	
Head Librarian, Australian Nuclear Science and Technology Organisation	
Senior Librarian, Hargrave Library, Monash University	
Library - Exchange Desk, National Institute of Standards and Technology, US	
Exchange Section, British Library Document Supply Centre	
Library, Chemical Abstracts Reference Service	
Engineering Societies Library, US	
Documents Librarian, The Center for Research Libraries, US	
Librarian - AMRL Sydney	2 copies
Army Scientific Adviser, Russell Offices - data sheet only	
Director General Force Development (Land) - data sheet only	
SO (Science), HQ 1 Division, Milpo, Enoggera, Qld 4057 - data sheet only	
Counsellor, Defence Science, Embassy of Australia - data sheet only	
Counsellor, Defence Science, Australian High Commission - data sheet only	
Scientific Adviser to DSTC Malaysia, c/- Defence Adviser - data sheet only	
Scientific Adviser to MRDC Thailand, c/- Defence Attache - data sheet only	
MHIPD	
MWSC PD	
Dr Ian Jones, MOD Sydney	
Mr J.T. Thompson, MOD Sydney	
Dr M. Hall, MOD Sydney	
Mr L. Hamilton, MOD Sydney	
Dr Martin Lawrence, MOD Sydney	
Dr Mark Readhead, MOD Sydney	
Dr D. Robinson, Ultrasonics Institute, CSIRO Division of Radiophysics, 126 Greville Street, Chatswood NSW 2467	
Dr David Blair, MOD Sydney	